

Anion Induced Formation of Supramolecular Associations Involving Lone pair– π and Anion– π Interactions in Co(II) Malonate Complexes: Experimental Observations, Hirshfeld Surface Analyses and DFT Studies

Prankrishna Manna,[†] Saikat Kumar Seth,[‡] Amrita Das,[†] Joanna Hemming,[§] Richard Prendergast,[§] Madeleine Helliwell,[§] Somnath Ray Choudhury,^{*,†} Antonio Frontera,^{||} and Subrata Mukhopadhyay^{*,†}

[†]Department of Chemistry, Jadavpur University, Kolkata 700 032, India

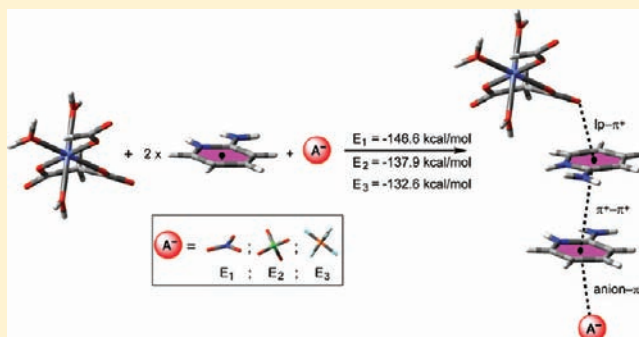
[‡]Department of Physics, M. G. Mahavidyalaya, Bhupatinagar, Midnapore (East), West Bengal 721 425, India

[§]School of Chemistry, The University of Manchester, Brunswick Street, Manchester, M13 9PL, United Kingdom

^{||}Departament de Química, Universitat de les Illes Balears, Crta. de Valldemossa km 7.5, 07122 Palma (Balears), Spain

Supporting Information

ABSTRACT: Three Co(II)–malonate complexes, namely, $(\text{C}_5\text{H}_7\text{N}_2)_4[\text{Co}(\text{C}_3\text{H}_2\text{O}_4)_2(\text{H}_2\text{O})_2](\text{NO}_3)_2$ (**1**), $(\text{C}_5\text{H}_7\text{N}_2)_4[\text{Co}(\text{C}_3\text{H}_2\text{O}_4)_2(\text{H}_2\text{O})_2](\text{ClO}_4)_2$ (**2**), and $(\text{C}_5\text{H}_7\text{N}_2)_4[\text{Co}(\text{C}_3\text{H}_2\text{O}_4)_2(\text{H}_2\text{O})_2](\text{PF}_6)_2$ (**3**) [$\text{C}_5\text{H}_7\text{N}_2$ = protonated 2-aminopyridine, $\text{C}_3\text{H}_4\text{O}_4$ = malonic acid, NO_3^- = nitrate, ClO_4^- = perchlorate, PF_6^- = hexafluorophosphate], have been synthesized from purely aqueous media, and their crystal structures have been determined by single crystal X-ray diffraction. A thorough analysis of Hirshfeld surfaces and fingerprint plots facilitates a comparison of intermolecular interactions in **1–3**, which are crucial in building supramolecular architectures. When these complexes are structurally compared with their previously reported analogous Ni(II) or Mg(II) compounds, a very interesting feature regarding the role of counteranions has emerged. This phenomenon can be best described as anion-induced formation of extended supramolecular networks of the type lone pair– $\pi/\pi-\pi/\pi-\pi$ –anion– π/π –lone pair and lone pair– $\pi/\pi-\pi/\pi-\pi$ –anion involving various weak forces like lone pair– π , $\pi-\pi$, and anion– π interactions. The strength of these π contacts has been estimated using DFT calculations (M06/6-31+G*), and the formation energy of the supramolecular networks has been also evaluated. The influence of the anion (NO_3^- , ClO_4^- , and PF_6^-) on the total interaction energy of the assembly is also studied.



INTRODUCTION

The world of noncovalent interactions has experienced dynamic growth in recent years.¹ Particularly, two new closely related potential supramolecular bonds involving anionic systems and electron-deficient aromatics, namely, the anion– π^2 and lone pair (lp)– π^3 interactions are clearly attracting increasing interest among chemists, physicists, theoreticians, and material scientists, most likely because anions are ubiquitous in chemical and biochemical processes. The tremendous progress achieved in this field of supramolecular chemistry is evidenced by mounting theoretical investigations⁴ and reports of solid-state structures.⁵ In a recent review, Gamez et al. examined future prospects of anion– π interactions for potential applications in anion recognition, and a pioneering Protein Data Bank search (PDB) inevitably revealed short anion– π contacts in some protein structures.⁶ This clearly demonstrates that such interactions will receive more attention in ensuing years with a quest for further experimental and theoretical studies to unravel the biological processes while enriching our understanding to the best possible extent.

During recent years, we have presented some good examples where anion– π and lone pair– π interactions are inextricably linked with the stabilization of molecules in the solid state.⁷ In this connection, we have also observed remarkable head-to-tail dimerization of heteroarenes like 2-amino-4-picoline^{7a,d,f,g} and 2-aminopyridine^{7a,c,f,g} induced by double lone pair– π noncovalent interactions. We have also energetically evaluated these noncovalent interactions and analyzed their mutual influences.^{7a,c,d,f,g} The computational results nicely complemented the experimental (structural) results, emphasizing the importance of the lone pair– $\pi/\pi-\pi/\pi-\pi$ –anion– π/π –lone pair and lone pair– $\pi/\pi-\pi/\pi-\pi$ –anion assemblies in the solid-state packing of hybrid inorganic–organic compounds investigated so far.

In the present study, three cobalt(II) malonate coordination complexes, namely, $(\text{C}_5\text{H}_7\text{N}_2)_4[\text{Co}(\text{C}_3\text{H}_2\text{O}_4)_2(\text{H}_2\text{O})_2](\text{NO}_3)_2$ (**1**), $(\text{C}_5\text{H}_7\text{N}_2)_4[\text{Co}(\text{C}_3\text{H}_2\text{O}_4)_2(\text{H}_2\text{O})_2](\text{ClO}_4)_2$ (**2**), and

Received: October 30, 2011

Published: February 22, 2012

(C₅H₇N₂)₄[Co(C₃H₂O₄)₂(H₂O)₂](PF₆)₂ (3) [where C₅H₇N₂ = protonated 2-aminopyridine, C₃H₂O₄ = malonic acid, NO₃⁻ = nitrate, ClO₄⁻ = perchlorate, and PF₆⁻ = hexafluorophosphate], have been synthesized and structurally characterized. These complexes were synthesized with the aim of investigating subtle changes in the self-assembly processes, where we have already witnessed the dynamic role played by some noncovalent interactions, by comparison with the structures of related nickel(II) and magnesium(II) complexes, *viz.*, (C₅H₇N₂)₄[M(II)-(C₃H₂O₄)₂(H₂O)₂](X)₂ [where M(II) = Ni/Mg and X = NO₃⁻/ClO₄⁻/PF₆⁻] reported earlier.^{7a,c,d,f,g} As anticipated, single-crystal X-ray structural analyses of compounds 1–3 revealed the generation of extended supramolecular networks by means of lone pair– π , π – π , and anion– π interactions of the type lone pair– π / π – π / π –anion– π / π –lone pair and lone pair– π / π – π / π –anion. In-depth structural analysis of the present complexes and judicious comparison with related ones demonstrates the importance of counteranions in inducing the formation of such supramolecular networks.

The Hirshfeld surface^{8–10} provides a remarkable way of exploring intermolecular interactions in molecular crystals using a partitioning of crystal space in a novel visual manner. The surfaces encode information about all intermolecular interactions and offer a facile way of obtaining information on crystal packing. The breakdown of the associated fingerprint plots¹¹ explores quantitatively the types of intermolecular contacts experienced by molecules and presents this information in a convenient color plot. This plot provides a useful means of revealing significant similarities and differences between related structures by analyzing the packing motifs. The size and shape of the Hirshfeld surface are intimately related to the chemical environment surrounding the molecule, making it ideal for use in comparing different crystal structures incorporating the same molecule. In the context of crystal structure prediction, Hirshfeld surface base tools shows a major advance in analyzing intermolecular interactions and should be considered by the crystal engineers in building molecular architectures. Investigation of Hirshfeld surface analyses for the three Co(II) complexes considering the asymmetric unit of the unit cell allows a detailed scrutiny of the comparison of weak forces experienced by each of these three complexes. The Hirshfeld surface and associated fingerprint plots have been presented to explore the nature of intermolecular interactions and their relative contributions in building the solid-state architecture.

In addition, we have carried out a theoretical DFT study in order to compute the binding energies associated with the noncovalent interactions observed in the crystal structures. Moreover, we have computed and compared the total formation energies of the lone pair– π / π – π / π –anion assemblies in order to analyze the influence of the anion (NO₃⁻/ClO₄⁻/PF₆⁻) on their global stability.

EXPERIMENTAL SECTION

Physical Measurements. IR spectra were recorded on a Perkin-Elmer RXI FT-IR spectrophotometer with the sample prepared as a KBr pellet, in the range 4000–600 cm⁻¹. Elemental analyses (C, H, N) were performed on a Perkin-Elmer 240C elemental analyzer.

Materials. All reactions were carried out under aerobic conditions and in water as the solvent. Malonic acid, cobalt(II) nitrate hexahydrate, cobalt(II) perchlorate hexahydrate, cobalt(II) chloride hexahydrate, 2-aminopyridine, ammonium hexafluorophosphate, sodium hydroxide, and all other chemicals were of reagent grade quality, purchased from Sigma-Aldrich Chemical Co. and used without further purification. Freshly boiled, doubly distilled water was used throughout the present investigation.

Synthesis of Compound 1. Cobalt(II) nitrate hexahydrate (0.291 g, 1.0 mmol) dissolved in 25 mL of water was allowed to react with malonic acid (0.208 g, 2.0 mmol) in water (25 mL) at 60 °C, resulting in a clear pink solution. A warm aqueous solution (20 mL) of 2-aminopyridine (0.376 g, 4.0 mmol) was added dropwise to the above solution with continuous stirring. The pH of the resulting solution was adjusted to 5.5 by the addition of dilute aqueous NaOH. The reaction mixture thus obtained was further heated at 60 °C for an hour with continuous stirring. The solution was then cooled to room temperature and filtered and left unperturbed for crystallization. After a few weeks, block shaped, pale orange single crystals suitable for X-ray analysis were obtained. The crystals were collected by filtration, washed with cold water, and dried in the air (yield: 65%). Anal. Calcd. for C₂₆H₃₆N₁₀O₁₆Co: C, 38.87; H, 4.39; N, 17.43%. Found: C, 38.76; H, 4.31; N, 17.34%. Main IR absorption bands observed for 1 (KBr pellet, cm⁻¹): 3330 (b), 3159 (b), 1681 (s), 1635 (s), 1573 (s), 1481 (s), 1433 (s), 1353 (b), 1161 (b), 1000 (s), 973 (s), 767 (s), 732 (b), 624 (s), 551 (s).

Synthesis of Compound 2. The synthesis of compound 2 was achieved using identical methods to those for compound 1 using cobalt(II) perchlorate hexahydrate (0.365 g, 1.0 mmol), malonic acid (0.208 g, 2.0 mmol), and 2-aminopyridine (0.376 g, 4.0 mmol). The resulting solution yielded block shaped, pink single crystals suitable for X-ray analysis after a few weeks. The crystals were collected by filtration, washed with cold water, and dried in the air (yield: 65%). Anal. Calcd. for C₂₆H₃₆N₈O₁₈Cl₂Co: C, 35.03; H, 4.16; N, 11.67%. Found: C, 34.89; H, 4.08; N, 11.56%. Main IR absorption bands observed for 2 (KBr pellet, cm⁻¹): 3409 (s), 3328 (b), 3147 (b), 1676 (m), 1633 (s), 1568 (s), 1481 (s), 1431 (s), 1353 (s), 1274 (s), 1247 (s), 1114 (b), 1085 (b), 999 (s), 973 (s), 933 (s), 767 (s), 729 (s), 626 (s), 551 (m).

Synthesis of Compound 3. Cobalt(II) chloride hexahydrate (0.237 g, 1.0 mmol) dissolved in 25 mL of water was allowed to react with malonic acid (0.208 g, 2.0 mmol) in water (25 mL) at 60 °C, resulting in a clear pink solution. A warm aqueous solution (20 mL) of 2-aminopyridine (0.376 g, 4.0 mmol) was added dropwise to the above solution with continuous stirring. Finally, a warm aqueous solution (20 mL) of ammonium hexafluorophosphate (0.652 g, 4.0 mmol) was added to it under stirring conditions. The pH of the resulting solution was adjusted to 5.4. The reaction mixture thus obtained was further heated at 60 °C for an hour with continuous stirring. The solution was then cooled to room temperature and filtered and left unperturbed for crystallization. After a few weeks, block shaped, orange single crystals suitable for X-ray analysis were obtained. The crystals were collected by filtration, washed with cold water, and dried in the air (yield: 60%). Anal. Calcd. for C₂₆H₃₆N₈O₁₀P₂F₁₂Co: C, 32.21; H, 3.71; N, 11.55%. Found: C, 32.10; H, 3.66; N, 11.46%. Main IR absorption bands observed for 3 (KBr pellet, cm⁻¹): 3610 (s), 3460 (s), 3311 (m), 3147 (b), 1679 (s), 1631 (s), 1566 (s), 1479 (s), 1431 (s), 1350 (s), 1247 (s), 1166 (s), 999 (s), 838 (s), 767 (s), 725 (m), 628 (s), 559 (s).

X-Ray Crystal Structure Determination of Complexes 1–3. X-ray diffraction data collection was carried out on a Bruker SMART APEX CCD diffractometer with graphite monochromated Mo K α radiation (λ = 0.71073 Å). The data were processed using SAINT¹² and corrected for absorption using SADABS.¹² The crystal structures were solved by direct methods using SHELXS-97¹² and refined by full-matrix least-squares on F^2 with SHELXL-97.¹² Other calculations were carried out using the SHELXTL package.¹² All hydrogen atoms were found by difference Fourier methods and refined isotropically. Data collection and refinement parameters for complexes 1–3 are summarized in Table 1.

Hirshfeld Surface Analysis. Molecular Hirshfeld surfaces^{8–10} in the crystal structure are constructed on the basis of the electron distribution calculated as the sum of spherical atom electron densities.¹³ For a given crystal structure and set of spherical atomic electron densities, the Hirshfeld surface is unique,¹⁴ and it is this property that suggests the possibility of gaining additional insight into the intermolecular interaction of molecular crystals. The Hirshfeld surface enclosing a molecule is defined by points where the contribution to the electron density from the molecule of interest is equal to the contribution from all of the other molecules. For each point on that isosurface, two distances are defined: d_w , the distance from the point to the nearest

Table 1. Crystallographic Data for Complexes 1, 2, and 3

| complex | 1 | 2 | 3 |
|---|--|---|--|
| formula | C ₂₆ H ₃₆ N ₁₀ O ₁₆ Co | C ₂₆ H ₃₆ N ₈ O ₁₈ Cl ₂ Co | C ₂₆ H ₃₆ N ₈ O ₁₀ P ₂ F ₁₂ Co |
| M | 803.58 | 878.46 | 969.50 |
| cryst syst | triclinic | triclinic | triclinic |
| space group | <i>P</i> $\bar{1}$ (No. 2) | <i>P</i> $\bar{1}$ (No. 2) | <i>P</i> $\bar{1}$ (No. 2) |
| <i>a</i> /Å | 7.0790(13) | 7.1122(7) | 7.1433(5) |
| <i>b</i> /Å | 10.7346(19) | 11.2696(10) | 11.7421(9) |
| <i>c</i> /Å | 11.415(2) | 11.7951(11) | 11.8894(9) |
| α | 89.405(4) | 86.908(2) | 84.313(1) |
| β | 85.886(3) | 84.168(2) | 84.263(1) |
| γ | 77.797(3) | 72.440(2) | 72.319(1) |
| <i>F</i> (000) | 417 | 453 | 493 |
| <i>V</i> /Å ³ | 845.6(3) | 896.41(15) | 942.90(12) |
| <i>Z</i> | 1 | 1 | 1 |
| <i>T</i> /K | 100 | 100 | 100 |
| θ min–max [deg] | 1.8–26.4 | 2.5–26.4 | 1.8–28.3 |
| λ (Mo <i>K</i> α)/Å | 0.71073 | 0.71073 | 0.71073 |
| μ (Mo <i>K</i> α)/mm ⁻¹ | 0.597 | 0.717 | 0.663 |
| cryst size [mm] | 0.18 × 0.20 × 0.30 | 0.40 × 0.40 × 0.50 | 0.20 × 0.50 × 0.50 |
| <i>R</i> ₁ , <i>I</i> > 2 σ (<i>I</i>) (all) | 0.0311 | 0.0309 | 0.0313 |
| <i>wR</i> ₂ , <i>I</i> > 2 σ (<i>I</i>) (all) | 0.0792 | 0.0808 | 0.0855 |
| S(GOF) | 1.06 | 0.99 | 1.03 |
| total reflns | 6739 | 5183 | 8224 |
| independent reflns (<i>R</i> _{int}) | 3397(0.020) | 3548(0.024) | 4299(0.020) |
| obsd data [<i>I</i> > 2 σ (<i>I</i>)] | 3098 | 3050 | 3995 |
| min. and max. resd. dens. [e/Å ³] | –0.27, 0.34 | –0.37, 0.42 | –0.28, 0.50 |

nucleus external to the surface, and d_i , the distance to the nearest nucleus internal to the surface. The normalized contact distance (d_{norm}) based on both d_e and d_i and the vdW radii of the atom, given by the eq 1, enable identification of the regions of particular importance to intermolecular interactions.⁸ The combination of d_e and d_i in the form of a 2D fingerprint plot¹¹ provides a summary of intermolecular contacts in the crystal.⁸ The Hirshfeld surfaces are mapped with d_{norm} , and 2D fingerprint plots presented in this paper were generated using CrystalExplorer 2.1.¹⁵ The 2D plots were created by binning (d_e , d_i) pairs in intervals of 0.01 Å and coloring each bin (essentially a pixel) of the resulting 2D histogram as a function of the fraction of surface points in that bin, ranging from blue (few points) through green to red (many points). Graphical plots of the molecular Hirshfeld surfaces mapped with d_{norm} using a red–white–blue color scheme, where red highlights shorter contacts, white is used for contacts around the vdW separation, and blue is for longer contacts. Moreover, two further colored properties based on the local curvature of the surface can be specified,¹⁶ e.g., shape index and curvedness.

$$d_{\text{norm}} = (d_i - r_i^{\text{vdw}})/r_i^{\text{vdw}} + (d_e - r_e^{\text{vdw}})/r_e^{\text{vdw}} \quad (1)$$

Theoretical Methods. The present theoretical study has been carried out using DFT calculations by means of the Gaussian 09 package.¹⁷ The level of theory is M06/6-31+G* for geometries and energies, which is an adequate compromise between the accuracy of the results and the size of the systems studied herein. The M06 functional is one of the most successful functionals for general applications and in particular for noncovalent interactions in chemical systems.¹⁸ To analyze the intermolecular interactions, the atoms-in-molecules (AIM) theory was employed.¹⁹ AIM is based upon those critical points where the gradient of the density, $\nabla\rho$, vanishes. Such points are classified by the curvature of the electron density; for example, a bond critical point has one positive curvature (in the internuclear direction) and two negative ones (perpendicular to the bond). Two bonded atoms are then connected with a bond path through the bond critical point. The properties evaluated at such bond critical points char-

acterize the bonding interactions. They have been widely used to study a great variety of molecular interactions.²⁰

RESULTS AND DISCUSSION

Crystal Structure Description of Complexes 1–3. The complexes (1–3) are essentially isomorphous and crystallized in the triclinic space group *P* $\bar{1}$ with the asymmetric unit consisting of half of the molecular anion [Co(C₃H₂O₄)₂(H₂O)₂]²⁻, two crystallographically independent C₅H₇N₂⁺ cations, and counteranions (a nitrate anion for 1, a perchlorate anion for 2, and a hexafluorophosphate anion for 3). The full anion is generated by the symmetry operation of an inversion center. Perspective views of the structures of complexes 1–3 are shown in Figure 1. Selected bond lengths, angles, and supramolecular interactions for complexes 1–3 are listed in Tables 2–7. In all of the complexes, cobalt(II) ions are located on an inversion center and possess an octahedral coordination environment whose equatorial planes are formed by the oxygen atoms O1 and O4 from the malonate units and their symmetry related counterparts O1**, O4** (** = 2 – *x*, 1 – *y*, 2 – *z*) from the second malonate units. Two water molecules (O5 and O5**, ** = 2 – *x*, 1 – *y*, 2 – *z*) occupy the *trans* axial positions, thus generating a CoO₄O'₂ chromophore. The Co–O bond distances in the equatorial plane vary between 2.0253(12) and 2.0554(10) Å. The value of the apical Co(1)–O(5) bond lengths varies between 2.1232(13) and 2.1257(15) Å, which is longer than the equatorial bond distances and suggests that the coordination polyhedron of the cobalt atoms in the anionic units is a slightly distorted octahedron. All coordination bonds and angles in the anionic unit are within the range of values previously observed for related malonate-containing complexes.^{7d,21} Malonate ligands usually adopt an envelope conformation in which only the methylene group is significantly displaced

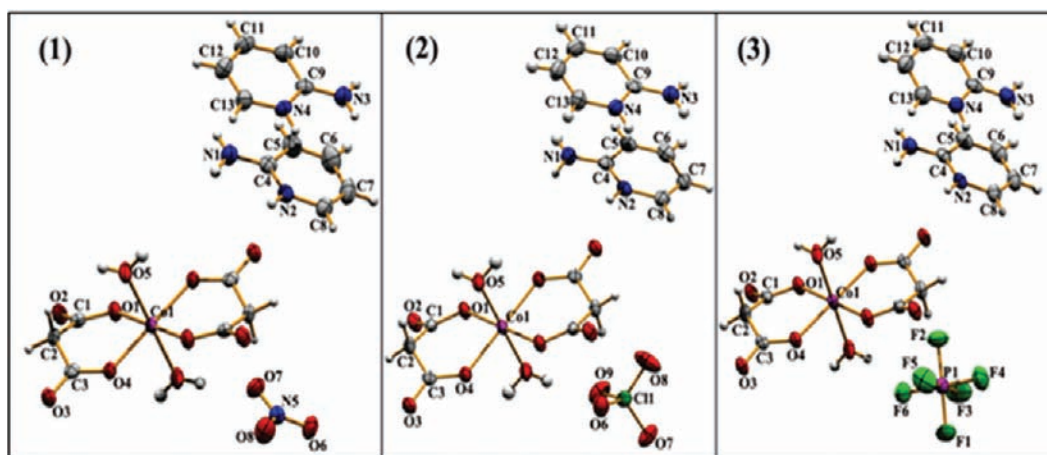


Figure 1. Representation (ORTEP) of the X-ray crystal structures of **1**, **2**, and **3**. Thermal ellipsoids are drawn at the 30% probability level. The unlabeled atoms in **1**, **2**, and in **3** are generated by the inversion operation ($2 - x, 1 - y, 2 - z$).

Table 2. Selected Bond Lengths (Angstroms) and Angles (degrees) for 1

| | | | |
|------------------------------|------------|-----------------|------------|
| Co(1)–O(1) | 2.0514(12) | O(4)–C(3) | 1.2805(19) |
| Co(1)–O(4) | 2.0253(12) | O(3)–C(3) | 1.233(2) |
| Co(1)–O(5) | 2.1251(14) | C(1)–C(2) | 1.518(2) |
| O(1)–C(1) | 1.2698(19) | C(2)–C(3) | 1.527(2) |
| O(2)–C(1) | 1.2487(19) | | |
| O(1)–Co(1)–O(4) | 88.67(5) | Co(1)–O(4)–C(3) | 128.54(10) |
| O(1)–Co(1)–O(5) | 92.41(5) | O(4)–C(3)–O(3) | 123.13(15) |
| O(1)–Co(1)–O(4) ^a | 91.33(5) | C(1)–C(2)–C(3) | 120.16(14) |
| O(1)–Co(1)–O(5) ^a | 87.59(5) | O(1)–C(1)–O(2) | 122.52(15) |
| O(4)–Co(1)–O(5) | 92.42(5) | O(4)–C(3)–C(2) | 119.45(14) |
| O(4)–Co(1)–O(5) ^a | 87.58(5) | O(1)–C(1)–C(2) | 119.35(13) |
| Co(1)–O(1)–C(1) | 128.24(10) | | |

^aSymmetry code: $2 - x, 1 - y, 2 - z$.

from the chelate ring plane, and the present examples are also in line with this generalization.^{7g,22}

The monomeric anionic units, that is, $[\text{Co}(\text{C}_3\text{H}_2\text{O}_4)_2(\text{H}_2\text{O})_2]^{2-}$, are interlinked to each other via strong self-complementary $\text{O5} \cdots \text{H1O5} \cdots \text{O2}$ hydrogen bonds which give rise to a $\text{R}_2^2(12)$ cyclic motif, ultimately generating an infinite 1D tape along the crystallographic a axis (Figure 2).

Each monomeric anionic unit also recognizes four aminopyridinium cations ($\text{C}_5\text{H}_7\text{N}_2^+$) through doubly coordinated carboxylate ends, leading to $\text{R}_2^2(8)$ hydrogen bonding assemblies involving different $\text{N} \cdots \text{H} \cdots \text{O}$ hydrogen bonding contacts

(Figure 3 and Tables 3, 5, and 7). Hydrogen bonding associations of dangling counteranions (nitrate, perchlorate, and hexafluorophosphate) with monomeric units in complexes **1–3** are shown in Figures 4–6.

The noncoordinating carbonyl oxygen atoms O3 of the malonate moieties in complexes **1–3** are orientated toward the π face of 2-aminopyridine rings (Figure 3). Distances between O3 atoms and the centroid of the aminopyridine rings are 3.114(2), 3.187(2), and 3.259(2) Å for complexes **1**, **2**, and **3** respectively (Table 8).

The angles with which these carbonyl oxygen atoms (O3) approach the π face of the aminopyridine ring reflect significant lone pair– π interaction.^{3b,7a,c,g} The shortest separation distances characterizing these interactions are, for complex **1**, $\text{O3} \cdots \text{C4} = 2.963(2)$ Å and $\text{O3} \cdots \text{N2} = 2.997(2)$ Å, for complex **2**, $\text{O3} \cdots \text{C4} = 2.979(2)$ Å and $\text{O3} \cdots \text{N2} = 3.049(2)$ Å, and for complex **3**, $\text{O3} \cdots \text{C4} = 3.030(3)$ Å and $\text{O3} \cdots \text{N2} = 3.053(3)$ Å, which are both below the sum of the corresponding van der Waals radii (sum of van der Waals radii of O and C is 3.22 Å, while that of O and N is 3.07 Å).^{3b,23} These 2-aminopyridine rings are further stacked over second aminopyridine molecules with an intercentroid separation of 4.092(2), 4.194(2), and 4.339(2) Å for complexes **1**, **2**, and **3**, respectively (Table 9). The amino nitrogen atoms N1 and N3 lie only 3.34 Å and 3.31 Å (complex **1**), 3.43 Å and 3.23 Å (complex **2**), and 3.47 Å and 3.27 Å (complex **3**) above the π face of the parallel-stacked 2-aminopyridine rings, revealing an unusual position of the $-\text{NH}_2$ group over the aromatic- π cloud. These coupled lone pair– π and π – π interactions within the monomeric units also assist the formation of a 1-D tape (Figure 3).

Table 3. Relevant H Bonds in Complex 1

| D–H···A | D–H [Å] | H···A [Å] | D···A [Å] | D–H···A [deg] | symmetry |
|--------------|---------|-----------|------------|---------------|-----------------------|
| N1–H2N1···O8 | 0.84(2) | 2.18(2) | 2.999(2) | 167(2) | $x, -1 + y, z$ |
| N3–H2N3···O3 | 0.85(2) | 2.01(2) | 2.847(2) | 173(2) | $-1 + x, y, z$ |
| N4–H1N4···O4 | 0.85(2) | 1.89(2) | 2.7280(19) | 171(2) | $-1 + x, y, z$ |
| N3–H1N3···O6 | 0.87(2) | 2.10(2) | 2.952(2) | 168(2) | $1 - x, 1 - y, 1 - z$ |
| O5–H2O5···O7 | 0.80(2) | 2.01(2) | 2.8048(19) | 170(2) | |
| O5–H1O5···O2 | 0.85(3) | 1.87(3) | 2.7067(19) | 171(2) | $1 + x, y, z$ |
| N1–H1N1···O2 | 0.83(2) | 2.11(2) | 2.938(2) | 172.5(19) | $1 - x, 1 - y, 2 - z$ |
| N2–H1N2···O1 | 0.84(2) | 1.93(2) | 2.7615(19) | 172(2) | $1 - x, 1 - y, 2 - z$ |
| C5–H5···O6 | 0.96(2) | 2.48(2) | 3.392(2) | 159.2(18) | $x, -1 + y, z$ |
| C7–H7···O3 | 0.90(2) | 2.36(2) | 3.202(2) | 154.7(19) | $1 - x, 1 - y, 1 - z$ |

Table 4. Selected Bond Lengths (Angstroms) and Angles (degrees) for 2

| | | | |
|------------------------------|------------|-----------------|------------|
| Co(1)–O(1) | 2.0540(13) | O(4)–C(3) | 1.280(2) |
| Co(1)–O(4) | 2.0337(12) | O(3)–C(3) | 1.234(2) |
| Co(1)–O(5) | 2.1257(15) | C(1)–C(2) | 1.517(3) |
| O(1)–C(1) | 1.271(2) | C(2)–C(3) | 1.524(3) |
| O(2)–C(1) | 1.251(2) | | |
| O(1)–Co(1)–O(4) | 88.95(5) | Co(1)–O(4)–C(3) | 129.29(11) |
| O(1)–Co(1)–O(5) | 93.81(5) | O(4)–C(3)–O(3) | 123.47(17) |
| O(1)–Co(1)–O(4) ^a | 91.05(5) | C(1)–C(2)–C(3) | 119.72(15) |
| O(1)–Co(1)–O(5) ^a | 86.20(5) | O(1)–C(1)–O(2) | 122.39(16) |
| O(4)–Co(1)–O(5) | 92.69(5) | O(4)–C(3)–C(2) | 119.49(15) |
| O(4)–Co(1)–O(5) ^a | 87.31(5) | O(1)–C(1)–C(2) | 118.99(18) |
| Co(1)–O(1)–C(1) | 127.89(11) | | |

^aSymmetry code: 2 – x, 1 – y, 2 – z.

These constitute the basic tenet of all of the complexes discussed so far, that is, formation of the monomeric [M(II)(mal)₂(H₂O)₂]^{2–} unit, their hydrogen bonded association in the 1D tape, and recognition of four aminopyridinium cations. Up to this stage, we have observed significant contributions from lone pair– π and π – π (actually NH₂– π) interactions, which further strengthen the 1D tapes. Different counteranions start playing their decisive roles after this stage. They have been found to take part in 2D and 3D assemblies along with other hydrogen bonds, and the resulting supramolecular networks are truly noteworthy. It is also very interesting that different counteranions produce different supramolecular networks, and henceforth this necessitates individual discussion of the complexes.

In the case of complex **1**, one dangling nitrate anion belonging to an adjacent monomeric unit (along the *b* axis) is in contact with this multilayered lone pair– π / π – π assembly from the open opposite face of the 2-aminopyridine ring (Tables 8 and 9). The shortest separation distance reflecting this anion– π interaction is N5...C10 = 3.122(3) Å, which is below the sum of the corresponding van der Waals radii (sum of van der Waals radii of N and C is 3.25 Å).²³ This generates a multilayered sandwich association of the type lone pair– π / π – π / π –anion, which is responsible for 2D assembly in **1** and is illustrated in Figure 7. The overall 3D association is mainly guided by two hydrogen bonds, that is, N1–H1N3...O6 and C7–H7...O3. Supramolecular associations involving lone pair– π and anion– π in **1** and earlier reported^{7f,g} Ni and Mg complexes are compared in detail in Figure 8.

Table 5. Relevant H Bonds in Complex 2

| D–H...A | D–H [Å] | H...A [Å] | D...A [Å] | D–H...A [deg] | symmetry |
|--------------|---------|-----------|-----------|---------------|---------------------|
| O5–H1O5...O2 | 0.91(3) | 1.78(3) | 2.687(2) | 178(3) | 1 + x, y, z |
| O5–H2O5...O6 | 0.79(2) | 2.05(2) | 2.839(2) | 177(3) | |
| N1–H1N1...O2 | 0.87(2) | 2.10(2) | 2.952(2) | 169.9(18) | 1 – x, 1 – y, 2 – z |
| N1–H2N1...O7 | 0.89(2) | 2.15(2) | 3.001(2) | 160(2) | x, –1 + y, z |
| N2–H1N2...O1 | 0.87(2) | 1.93(2) | 2.788(2) | 170(2) | 1 – x, 1 – y, 2 – z |
| N3–H1N3...O8 | 0.85(2) | 2.18(2) | 3.024(2) | 171(2) | 1 – x, 1 – y, 1 – z |
| N3–H2N3...O3 | 0.89(3) | 1.93(2) | 2.818(2) | 177(2) | –1 + x, y, z |
| N4–H1N4...O4 | 0.85(2) | 1.93(2) | 2.768(2) | 169(2) | –1 + x, y, z |
| C2–H2B...O6 | 0.93(2) | 2.59(2) | 3.491(3) | 162(2) | |
| C5–H5...O7 | 0.94(2) | 2.59(2) | 3.352(3) | 138.5(17) | x, –1 + y, z |
| C7–H7...O3 | 0.91(2) | 2.48(2) | 3.182(2) | 134.2(16) | 1 – x, 1 – y, 1 – z |

Table 6. Selected Bond Lengths (Angstroms) and Angles (degrees) for 3

| | | | |
|------------------------------|------------|-----------------|------------|
| Co(1)–O(1) | 2.0554(10) | O(4)–C(3) | 1.2826(18) |
| Co(1)–O(4) | 2.0274(10) | O(3)–C(3) | 1.2370(17) |
| Co(1)–O(5) | 2.1232(13) | C(1)–C(2) | 1.5201(19) |
| O(1)–C(1) | 1.2712(18) | C(2)–C(3) | 1.524(2) |
| O(2)–C(1) | 1.2509(18) | | |
| O(1)–Co(1)–O(4) | 89.40(4) | Co(1)–O(4)–C(3) | 130.33(9) |
| O(1)–Co(1)–O(5) | 94.07(4) | O(4)–C(3)–O(3) | 123.20(13) |
| O(1)–Co(1)–O(4) ^a | 90.60(4) | C(1)–C(2)–C(3) | 120.50(12) |
| O(1)–Co(1)–O(5) ^a | 85.93(4) | O(1)–C(1)–O(2) | 122.12(12) |
| O(4)–Co(1)–O(5) | 93.38(4) | O(4)–C(3)–C(2) | 119.87(12) |
| O(4)–Co(1)–O(5) ^a | 86.62(4) | O(1)–C(1)–C(2) | 119.82(13) |
| Co(1)–O(1)–C(1) | 128.46(9) | | |

^aSymmetry code: 2 – x, 1 – y, 2 – z.

In the case of **2**, one perchlorate anion from an adjacent monomeric unit along the *a* axis is sandwiched between two aminopyridine rings by means of anion– π contacts involving the oxygen atoms O7 and O8, resulting in a π –anion– π type interaction. The shortest separation distances illustrating these interactions are O7...C9 = 3.214(3), O7...C10 = 3.123(3), and O8...C6 = 3.224(3) Å, which are either below or equal to the sum of the corresponding van der Waals radii (sum of van der Waals radii of O and C is 3.22 Å).²³ The aminopyridine ring, which is involved in very weak anion– π contact with the perchlorate oxygen atom O8, is further interacting with the oxygen atom O3 from another malonate moiety (lone pair– π association). The entire supramolecular assembly exhibits an exceptional combination of lone pair– π , π – π , and anion– π interactions, which can be best designated as a lone pair– π / π – π / π –anion– π / π –lone pair network (Figure 9). In this assembly, one anion– π interaction is very long (4.08 Å from oxygen to ring centroid) with a very narrow angle with respect to the aromatic plane, as can be appreciated in Figure 9. This issue deserves special attention and will be further studied below in the theoretical part.

Compound **2** represents a unique combination of weak forces in the solid-state structure that contributes to the self-assembly process. This network along with other hydrogen bonds (N1–H2N1...O7 and N3–H1N3...O8) is responsible for the overall three-dimensional packing of the complex. Supramolecular associations involving lone pair– π and weaker anion– π in **2** and earlier reported^{7f,g} Ni and Mg complexes are compared in detail in Figure 10.

Table 7. Relevant H Bonds in Complex 3

| D–H...A | D–H [Å] | H...A [Å] | D...A [Å] | D–H...A [deg] | symmetry |
|--------------|---------|-----------|------------|---------------|---------------------|
| O5–H1O5...O2 | 0.80(3) | 1.88(3) | 2.6737(17) | 172(2) | 1 + x, y, z |
| O5–H2O5...F5 | 0.78(2) | 2.36(2) | 3.0681(18) | 152(2) | |
| O5–H2O5...F6 | 0.78(2) | 2.25(2) | 2.9381(17) | 149(2) | |
| N1–H1N1...O2 | 0.85(2) | 2.10(2) | 2.9409(17) | 175(2) | 1 – x, 1 – y, 2 – z |
| N1–H2N1...F1 | 0.89(2) | 2.12(2) | 2.9829(17) | 162.7(19) | x, –1 + y, z |
| N2–H1N2...O1 | 0.83(2) | 2.01(2) | 2.8287(16) | 167(2) | 1 – x, 1 – y, 2 – z |
| N3–H1N3...F3 | 0.83(2) | 2.13(2) | 2.9239(19) | 161(2) | 1 – x, 1 – y, 1 – z |
| N3–H2N3...O3 | 0.86(2) | 1.97(2) | 2.8155(19) | 171(2) | –1 + x, y, z |
| N4–H1N4...O4 | 0.85(2) | 1.93(2) | 2.7737(17) | 176.0(19) | –1 + x, y, z |
| C2–H2B...F5 | 0.97(2) | 2.37(2) | 3.285(2) | 157.2(17) | |
| C7–H7...O3 | 0.91(2) | 2.56(2) | 3.2760(19) | 135.9(17) | 1 – x, 1 – y, 1 – z |
| C8–H8...F2 | 0.94(2) | 2.53(2) | 3.3291(19) | 143.4(15) | –1 + x, y, z |
| C13–H13...F5 | 0.94(2) | 2.47(2) | 3.332(2) | 152.4(17) | 1 – x, 1 – y, 2 – z |

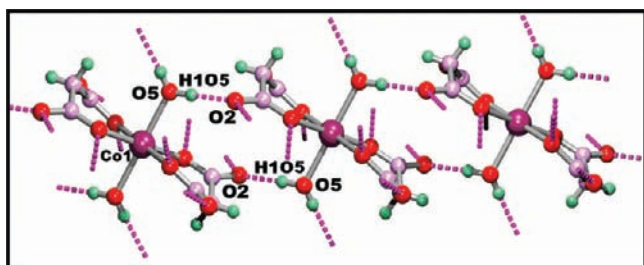


Figure 2. Formation of 1D tape in complexes 1–3 through association of discrete $[\text{Co}(\text{mal})_2(\text{H}_2\text{O})_2]^{2-}$ monomeric units. The occurrence of hydrogen bonding interactions ($\text{O5}-\text{H1O5}\cdots\text{O2}$) along the a axis generates a $R_2^2(12)$ cyclic motif.

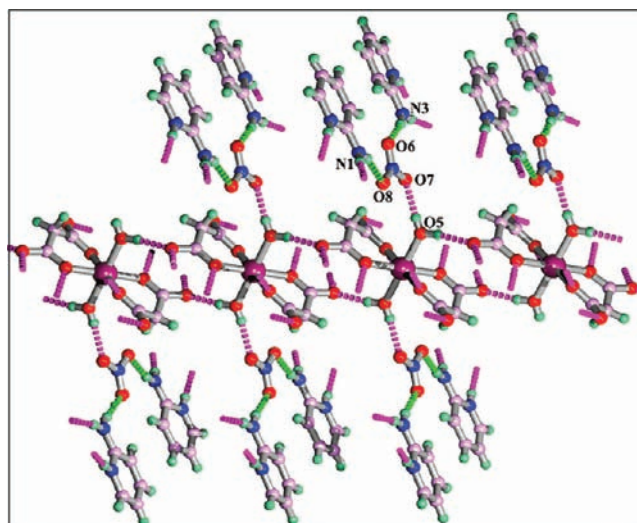


Figure 4. Illustration of two dangling nitrate ions being connected with the monomeric $[\text{Co}(\text{mal})_2(\text{H}_2\text{O})_2]^{2-}$ unit of 1 through $\text{O5}-\text{H2O5}\cdots\text{O7}$ hydrogen bonds. Each nitrate ion is also hydrogen bonded with two aminopyridine molecules.

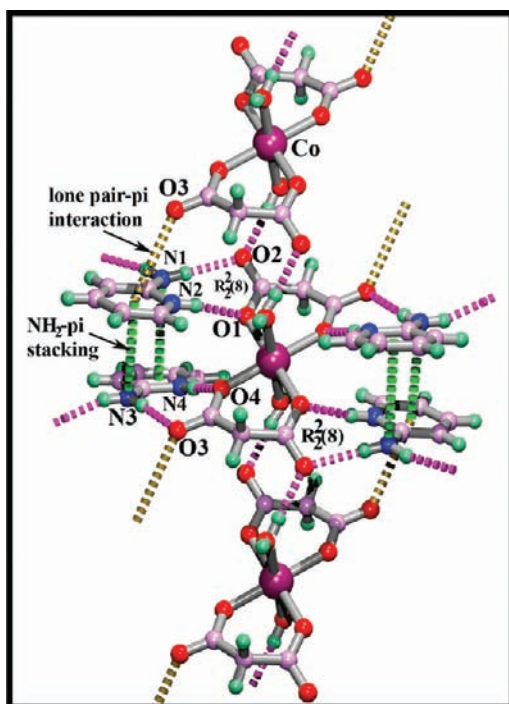


Figure 3. Illustration of each monomeric unit of complexes 1–3 also being connected to four 2-aminopyridinium cations through the formation of $R_2^2(8)$ cyclic motifs. The chain is viewed along the b axis.

In the case of 3, one fluorine atom (F1) of the PF_6^- anion from an adjacent monomeric unit along the b axis makes an anion– π contact with one of the open opposite faces of the two

stacked 2-aminopyridine rings [$\text{F1}\cdots\text{Cg} = 3.616(3)$ Å]. The shortest separation distance reflecting this interaction is $\text{F1}\cdots\text{C10} = 3.009$ Å, which is below the sum of the corresponding van der Waals radii²³ (sum of van der Waals radii of F and C is 3.17 Å). Thus, an elegant association of various weak forces is generated, which can be best described as a lone pair– $\pi/\pi-\pi/\pi-\pi$ -anion interaction. Such a unique multilayered lone pair– $\pi/\pi-\pi/\pi-\pi$ -anion interaction is found to contribute to the formation of the 2D assembly in 3 (Figure 11), and this has been only recently explored by us in similar Ni(II) and Mg(II) complexes, i.e., $(\text{C}_5\text{H}_7\text{N}_2)_4[\text{M}(\text{II})(\text{mal})_2(\text{H}_2\text{O})_2](\text{NO}_3)_2$ and $(\text{C}_5\text{H}_7\text{N}_2)_4[\text{M}(\text{II})(\text{mal})_2(\text{H}_2\text{O})_2](\text{PF}_6)_2$ [$\text{M} = \text{Mg}(\text{II})^{7f}/\text{Ni}(\text{II})^{7g}$], and where this sandwich association plays a similar role in the formation of a 2D assembly.^{7g} The overall 3-D association in 3 is mainly guided by the hydrogen bonds $\text{N3}-\text{H1N3}\cdots\text{F3}$ and $\text{N1}-\text{H2N1}\cdots\text{F1}$. Supramolecular associations involving lone pair– π and anion– π in 3 and earlier reported^{7f,g} Ni and Mg complexes are compared in detail in Figure 12.

These complexes clearly illustrate how counteranions play an important role in the 2D and 3D packing of metal organic hybrid frameworks by the formation of extended supramolecular networks. It is also interesting that nitrate and hexafluorophosphate

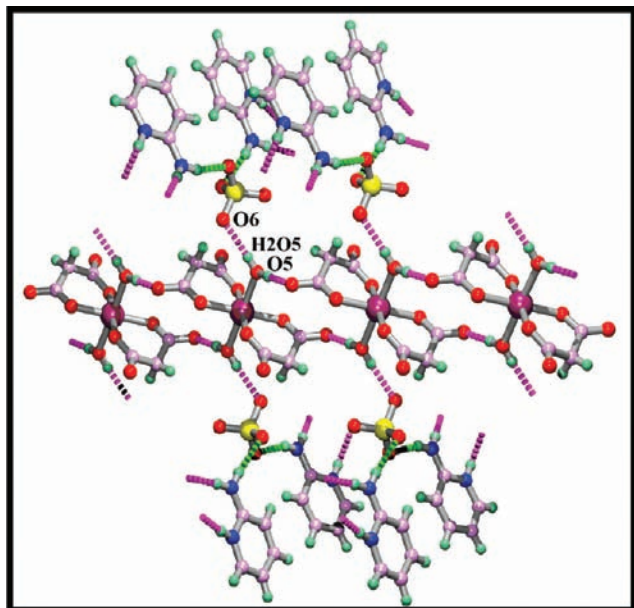


Figure 5. Illustration of two dangling perchlorate ions being connected with the monomeric $[\text{Co}(\text{mal})_2(\text{H}_2\text{O})_2]^{2-}$ unit of **2** through $\text{O5-H2O5}\cdots\text{O6}$ hydrogen bonds. Each perchlorate ion is also hydrogen bonded with two aminopyridine molecules.

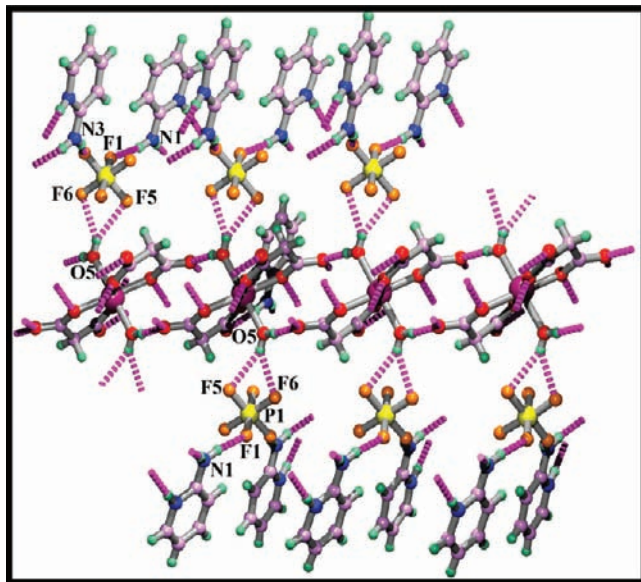


Figure 6. Illustration of two dangling hexafluorophosphate ions being connected with the monomeric $[\text{Co}(\text{mal})_2(\text{H}_2\text{O})_2]^{2-}$ unit of **3** through $\text{O5-H2O5}\cdots\text{F5}$ and $\text{O5-H2O5}\cdots\text{F6}$ hydrogen bonds. Each hexafluorophosphate ion is also hydrogen bonded with two aminopyridine molecules.

become attached with electron deficient aminopyridinium cations in the same fashion, whereas perchlorate used multiple arms for the same purpose and generated different network than the others. This is illustrated in Table 10. For perchlorate complexes, it is also noteworthy that only in the case of the Mg complex did this anion form a minimum separation and, due to this unusual perchlorate \cdots perchlorate interaction, result in the creation of 2D sheets.^{7f}

Hirshfeld Surfaces. The Hirshfeld surfaces of **1–3** are illustrated in Figure 13, showing surfaces that have been mapped

over a d_{norm} range of -0.5 to 1.5 Å, a shape index of -1.0 to 1.0 Å, and curvedness of -4.0 to 0.4 Å. The surfaces are shown as transparent to allow visualization of the molecular moiety, in a similar orientation for all of the structures, around which they were calculated. We have considered the asymmetric unit among the entire unit cell for all of the complexes. The information present in the hydrogen bonding tables is summarized effectively in the spots, with the large circular depressions (deep red) visible on the d_{norm} surfaces indicative of hydrogen bonding contacts, and other visible spots are due to $\text{H}\cdots\text{H}$ contacts. The dominant $\text{O}\cdots\text{H}$ interactions in the title complexes can be viewed in Hirshfeld surface plots by the bright red area in Figure 13. The light red spots are due to $\text{C-H}\cdots\text{O}$ interactions (Figure 13). The small extent of area and light color on the surface indicates weaker and longer contacts other than hydrogen bonds.

The $\text{O-H}\cdots\text{O}$ intermolecular interactions appear as two distinct spikes of almost equal length in the 2D fingerprint plots (Figure 14) in the region 1.67 Å $< (d_e + d_i) < 1.72$ Å. Complementary regions are visible in the fingerprint plots where one molecule acts as a donor ($d_e > d_i$) and the other as an acceptor ($d_e < d_i$). The fingerprint plots can be decomposed to highlight particular atom pair close contacts.^{13a} This decomposition enables the separation of contributions from different interaction types, which overlap in the full fingerprint. The Hirshfeld surface analysis does not show a similar proportion of $\text{O}\cdots\text{H}$ interactions for each molecule, ranging from 21.5% to 35.7%. In all cases, the $\text{O}\cdots\text{H}$ interactions are represented by a spike in the bottom left (donor) area, whereas the $\text{H}\cdots\text{O}$ interactions are represented by a spike in the bottom right region in the fingerprint plot. The proportion of $\text{H}\cdots\text{O}$ interactions has a larger variety than its $\text{O}\cdots\text{H}$ counterparts, ranging from 11.1% to 26.0%.

The proportions of $\text{O}\cdots\text{H}/\text{H}\cdots\text{O}$ interactions comprise 58.1%, 61.7%, and 32.6% of the total Hirshfeld surface for each molecule of **1**, **2**, and **3**, respectively. The points in the (d_i , d_e) regions of (1.03 Å, 0.65 Å) in the Fingerprint plots are due to $\text{O-H}\cdots\text{O}$ interactions (Figure 14) and represent the water oxygen interacting with carbonyl oxygen, forming a centrosymmetric $\text{R}_2^2(12)$ hydrogen bonding motif leading to the formation of 1D tape in **1–3**. The $\text{H}\cdots\text{O}$ interactions where the carbonyl oxygen acts as an acceptor to the H atoms of the NH groups represent the closest contacts in the structures and can be viewed as a pair of large red spots on the d_{norm} surface (Figure 13). The $\text{H}\cdots\text{O}$ interaction represented by the spike illustrates that each anionic unit of the title compounds is in contact with the aminopyridinium cations through doubly coordinated carboxylate ends, leading to $\text{R}_2^2(8)$ hydrogen bonding assemblies involving the $\text{N-H}\cdots\text{O}$ hydrogen bonds. The $\text{N}\cdots\text{H}$ interactions comprise 2.6, 1.6, and 0.3% of the Hirshfeld surfaces for each molecule of **1**, **2**, and **3**, respectively. No significant $\text{C-H}\cdots\pi$ interaction has been observed for **1–3**, with C-H close contacts varying from 4.4% in **2** to 4.9% in **3**. A significant difference between the molecular interactions in **1–3** in terms of $\text{H}\cdots\text{H}$ interactions is reflected in the distribution of scattered points in the fingerprint plots, which spread only up to $d_i = d_e = 1.126$ Å in **1**, $d_i = d_e = 1.131$ Å in **2**, and $d_i = d_e = 1.136$ Å in **3**.

The inspection of contacts between other atom types pointed out that there are also specific features of the $\text{C}\cdots\text{O}/\text{O}\cdots\text{C}$ interactions in the fingerprint plots (Figure 14) for all of the complexes. The clear green/blue lines with the shortest ($d_e + d_i$) ≈ 3.2 Å in **1**, ($d_e + d_i$) ≈ 3.1 Å in **2**, and ($d_e + d_i$) ≈ 3.3 Å in **3** correspond to carbonyl (lone pair) interactions. It is worth noting that in the

Table 8. Geometrical Parameters (Å, deg) for the Lone Pair... π /Anion... π Interactions for the Title Complexes^a

| Y–X(I)...Cg(J) | X...C(g) | Y...C(g) | Y–X...C(g) | X–Perp | symmetry |
|----------------|----------|----------|------------|--------|-------------------|
| complex 1 | | | | | |
| C3–O3...Cg(1) | 3.114(2) | 4.025(2) | 130.45(10) | 2.905 | x, y, z |
| N5–O8...Cg(2) | 3.465(2) | 3.639(2) | 87.91(9) | –3.379 | $1 + x, 1 + y, z$ |
| complex 2 | | | | | |
| C3–O3...Cg(1) | 3.187(2) | 4.120(2) | 132.30(13) | 2.936 | x, y, z |
| Cl1–O8...Cg(1) | 4.079(2) | 5.473(2) | 163.63(11) | 2.804 | x, y, z |
| complex 3 | | | | | |
| C3–O3...Cg(1) | 3.259(2) | 4.238(2) | 136.11(9) | 2.964 | x, y, z |

^aCg(1) and Cg(2) are the centroids of the (N2, C4–C8) and (N4, C9–C13) rings, respectively.

Table 9. Geometrical Parameters (Å, deg) for the π -Stacking Moieties Involved in the π - π Interactions for the Title Complexes^a

| rings I – J | Rc ^b | R1v ^c | R2v ^d | α | β | γ | symmetry |
|---------------|-----------------|------------------|------------------|----------|---------|----------|-----------|
| complex 1 | | | | | | | |
| Cg(1)...Cg(2) | 4.092(2) | 3.2685(8) | –3.2461(8) | 5.7(1) | 37.50 | 36.98 | x, y, z |
| complex 2 | | | | | | | |
| Cg(1)...Cg(2) | 4.194 (2) | 3.168(1) | –3.369(1) | 7.2(1) | 36.56 | 40.94 | x, y, z |
| complex 3 | | | | | | | |
| Cg(1)...Cg(2) | 4.339(2) | 3.186(1) | –3.412(1) | 11.5(1) | 38.16 | 42.77 | x, y, z |

^aCg(1) and Cg(2) are the centroids of the (N2, C4–C8) and (N4, C9–C13) rings, respectively. ^bCentroid distance between ring I and ring J. ^cVertical distance from ring centroid I to ring J. ^dVertical distance from ring centroid J to ring I.

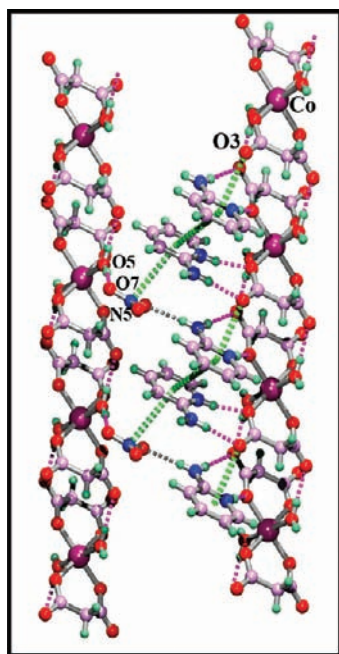


Figure 7. Two-dimensional assembly of monomeric units of **1** via lone pair- π / π - π - π -anion interactions. This extended network is shown in green dotted lines. This assembly is viewed along the c axis.

crystal of **3** those contacts are much more dispersed, are significantly longer, and cover only 1.7% of the Hirshfeld surface compared to 2.9% in **1** and 3.6% in **2**. The relative contributions of the different interactions to the Hirshfeld surfaces were calculated for **1**–**3** (Figure 15). From the Hirshfeld surfaces, it is clear that the aminopyridinium moieties of the title complexes are related to one another where, above the plane of the molecule, inspection of the adjacent red and blue triangles on the shape index surface shows that the π - π stacking interaction is almost identical in all of the crystal structures.

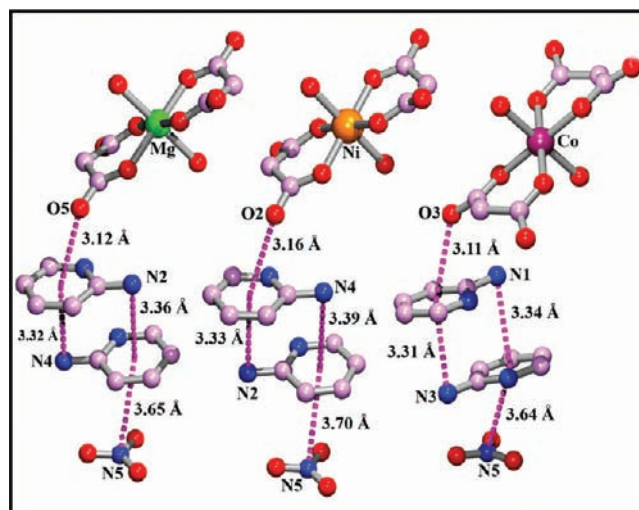


Figure 8. Comparison of supramolecular associations (lone pair- π / π - π / π -anion) found in Mg, Ni, and Co complexes. Hydrogen atoms are omitted for clarity.

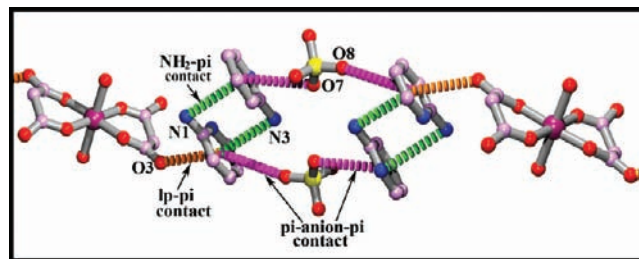


Figure 9. Supramolecular network in **2**, generated by lone pair- π / π - π / π -anion- π / π -lone pair interactions. Hydrogen atoms are omitted for clarity.

The presence of π - π stacking is evident because of a flat region toward the bottom of both sides of the molecules and is clearly

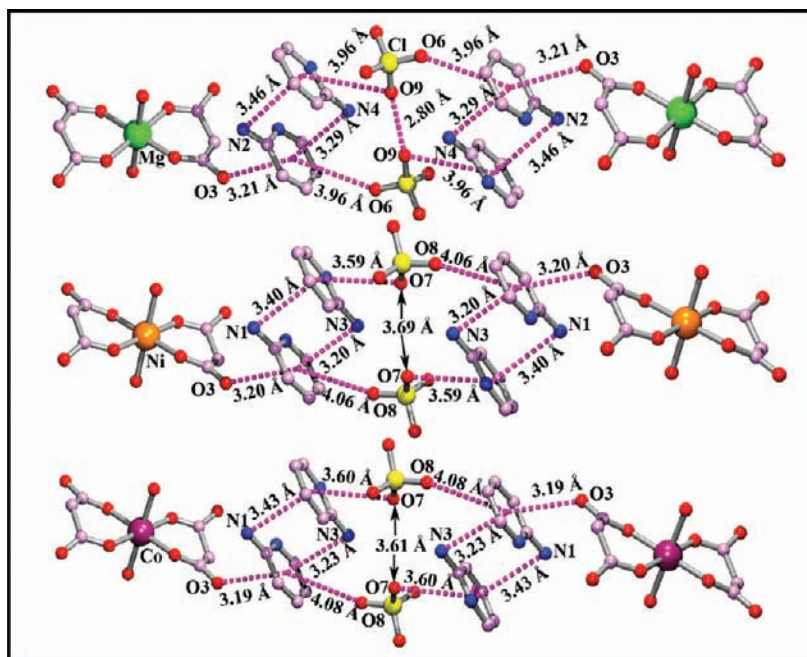


Figure 10. Comparison of supramolecular associations (lone pair- π/π - π/π -anion- π/π -lone pair) found in Mg, Ni, and Co complexes. Hydrogen atoms are omitted for clarity.

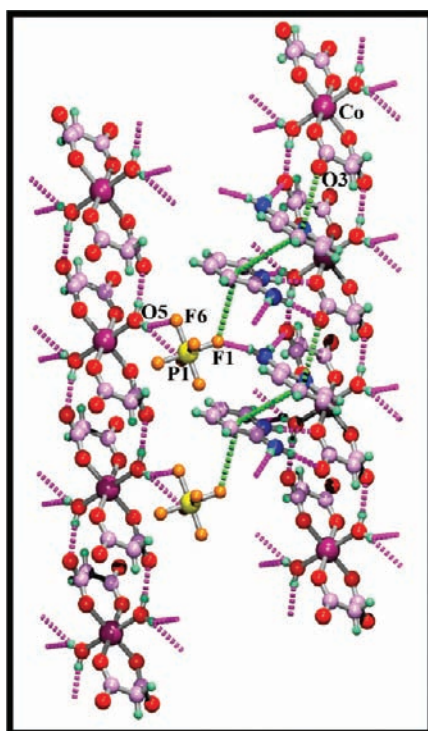


Figure 11. Two-dimensional assembly of monomeric units of **3** via lone pair- π/π - π/π -anion interactions. This extended network is shown in green dotted lines. This assembly is viewed along the c axis.

visible on the curvedness surface (Figure 13). On the d_e surface, this feature appears as a relatively flat green region, where the contact distances are all very similar. The corresponding fingerprint plot in Figure 14 shows this interaction as a region of blue/green color on the diagonal around $d_e \approx d_i \approx 1.90$ Å, $d_e \approx d_i \approx 1.84$ Å, and $d_e \approx d_i \approx 1.78$ Å for complexes **1**, **2**, and **3**, respectively. The pattern of red and blue triangles on the same

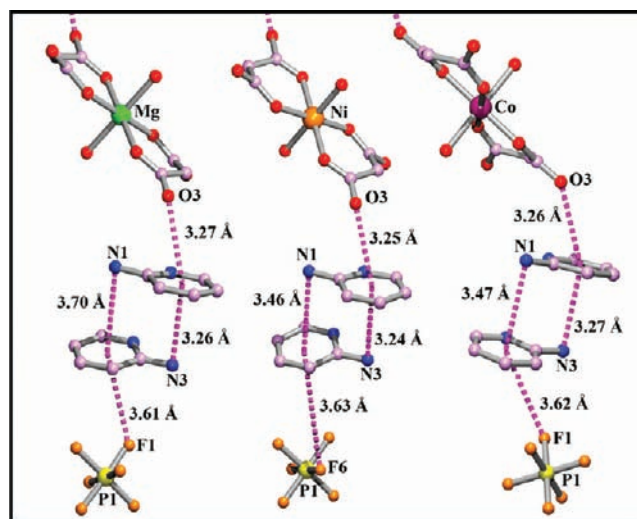


Figure 12. Comparison of supramolecular associations (lone pair- π/π - π/π -anion) found in Mg, Ni, and Co complexes. Hydrogen atoms are omitted for clarity.

Table 10. Supramolecular Networks As Found in Different Complexes

| complexes | observed network |
|---|---|
| $(C_5H_7N_2)_4[M(II)(C_3H_2O_4)_2(H_2O)_2]$ (NO_3) ₂ | lone pair- π/π - π/π -anion |
| $M(II) = Mg/Ni/Co$ | |
| $(C_5H_7N_2)_4[M(II)(C_3H_2O_4)_2(H_2O)_2]$ (ClO_4) ₂ | lone pair- π/π - π/π -anion- π/π - lone pair |
| $M(II) = Mg/Ni/Co$ | |
| $(C_5H_7N_2)_4[M(II)(C_3H_2O_4)_2(H_2O)_2]$ (PF_6) ₂ | lone pair- π/π - π/π -anion |
| $M(II) = Mg/Ni/Co$ | |

region of the shape index surface (Figure 13) is characteristic of π - π stacking and is used to determine the way in which the

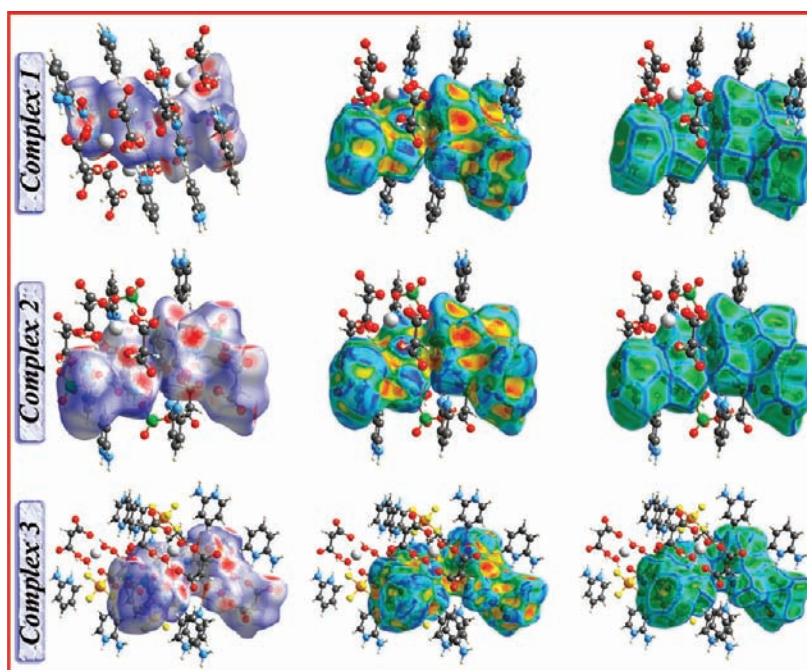


Figure 13. Hirshfeld surfaces mapped with d_{norm} (left), shape index (middle), and curvedness (right) for complexes 1–3.

molecules overlap and make contact with each other. The pattern of red and blue triangles on this region of both sides of the molecule shows how adjacent molecules in the crystal are related by translation. Blue triangles represent convex regions due to ring carbon atoms of the molecule inside the surface, while red triangles represent concave regions due to carbon atoms of the π stacked molecule above it. Figure 15 contains the percentages of contributions for a variety of contacts in the complexes 1–3. From these values, one can see that the other interactions are minimal in 2 (only 1.6% of the total Hirshfeld surface area compared with 2.3% and 37.6% in 1 and 3, respectively). In 3, the F \cdots H/H \cdots F interactions comprise 32.6% of the total Hirshfeld surface area, which has been included as other interactions. This quantitatively verifies observations that are obvious from inspecting the different structures. This conclusion is further evident from the shape of the blue outline on the curvedness surface (Figure 13), which unambiguously delineates contacting patches of the molecules.

Theoretical Study. We have performed a computational study using DFT calculations to analyze the noncovalent interactions involved in the interesting 3D architectures of compounds 1–3, focusing our attention on the influence of the anion in the interaction energies of the anion– π / π – π /anion– π assemblies. This supramolecular association is very common in a variety of $(\text{C}_5\text{H}_7\text{N}_2)_4[\text{M}(\text{II})(\text{C}_3\text{H}_2\text{O}_4)_2(\text{H}_2\text{O})_2](\text{X})$ complexes ($\text{X} = \text{NO}_3^-$, ClO_4^- , and PF_6^- ; $\text{M} = \text{Ni}$, Mg , and Co), as has been analyzed and discussed in the Experimental Section. The robustness of this assembly should be emphasized, since it is maintained for anions of different natures, sizes, and geometries and different metal ions as well. Before presenting the results, some considerations should be made regarding the theoretical model used in the calculations. We have mainly studied the anion– π / π – π /anion– π assembly observed in the crystal structures of compounds 1–3. This fragment of the crystal has been slightly modified in order to be neutral. It is important to be as realistic as possible, to evaluate the formation energy of the assembly and the strength of the different

interactions. Obviously, the neutral structures 1–3 are composed of several charged subunits, namely, nitrate, perchlorate, or hexafluorophosphate anions; the $[\text{Co}(\text{C}_3\text{H}_2\text{O}_4)_2(\text{H}_2\text{O})_2]^{2-}$ dianion; and protonated 2-aminopyridine. The $[\text{Co}(\text{C}_3\text{H}_2\text{O}_4)_2(\text{H}_2\text{O})_2]^{2-}$ dianion has been used to adjust the charge of the assembly, replacing a bidentate malonate ligand with a monodentate formate ligand and a water molecule. This approximation is supported by the fact that each $[\text{Co}(\text{C}_3\text{H}_2\text{O}_4)_2(\text{H}_2\text{O})_2]^{2-}$ dianion interacts with two sets of stacked 2-aminopyridine moieties (see Experimental Section), and in the crystal fragment in which we have chosen to perform the theoretical study, only one set is used. Another point that should be analyzed before discussing the results is that the $[\text{Co}(\text{C}_3\text{H}_2\text{O}_4)_2(\text{H}_2\text{O})_2]^{2-}$ moiety is dianionic; therefore, the lp– π interactions described hitherto in the manuscript are energetically very favored due to electrostatic effects because the lp donor molecule is negatively charged. As a matter of fact, the lp– π interactions involving the $[\text{Co}(\text{C}_3\text{H}_2\text{O}_4)_2(\text{H}_2\text{O})_2]^{2-}$ moiety could be considered as anion– π interactions; however, the lp– π nomenclature has been maintained because, formally, it is the lone pair of the carbonyl group of the malonate that participates in the interaction.

We have computed, at the M06/6-31+G* level of theory, the formation energies of the anion– π / π – π /anion– π assemblies of 1–3 (Figure 16). It can be observed that the formation energies of the assemblies are in all cases large and negative, indicating that its formation is very favorable. In addition, the binding energy of compound 1 (E_1) is the most favorable, followed by the binding energy of compound 2 (E_2 (rel) = 8.2 kcal/mol) and finally compound 3, which presents a relative binding energy of 13.5 kcal/mol. The large binding energy of the assemblies is a consequence of the ionic nature of the interacting parts. That is the reason why we have denoted the π system as π^+ in the figure. The π^+ – π^+ stacking is expected to be repulsive because it is electrostatically very unfavorable (the intermolecular π^+ – π^+ indicated in Figure 16 corresponds to the intercentroid distance). As reported before by some of us^{7f,g}

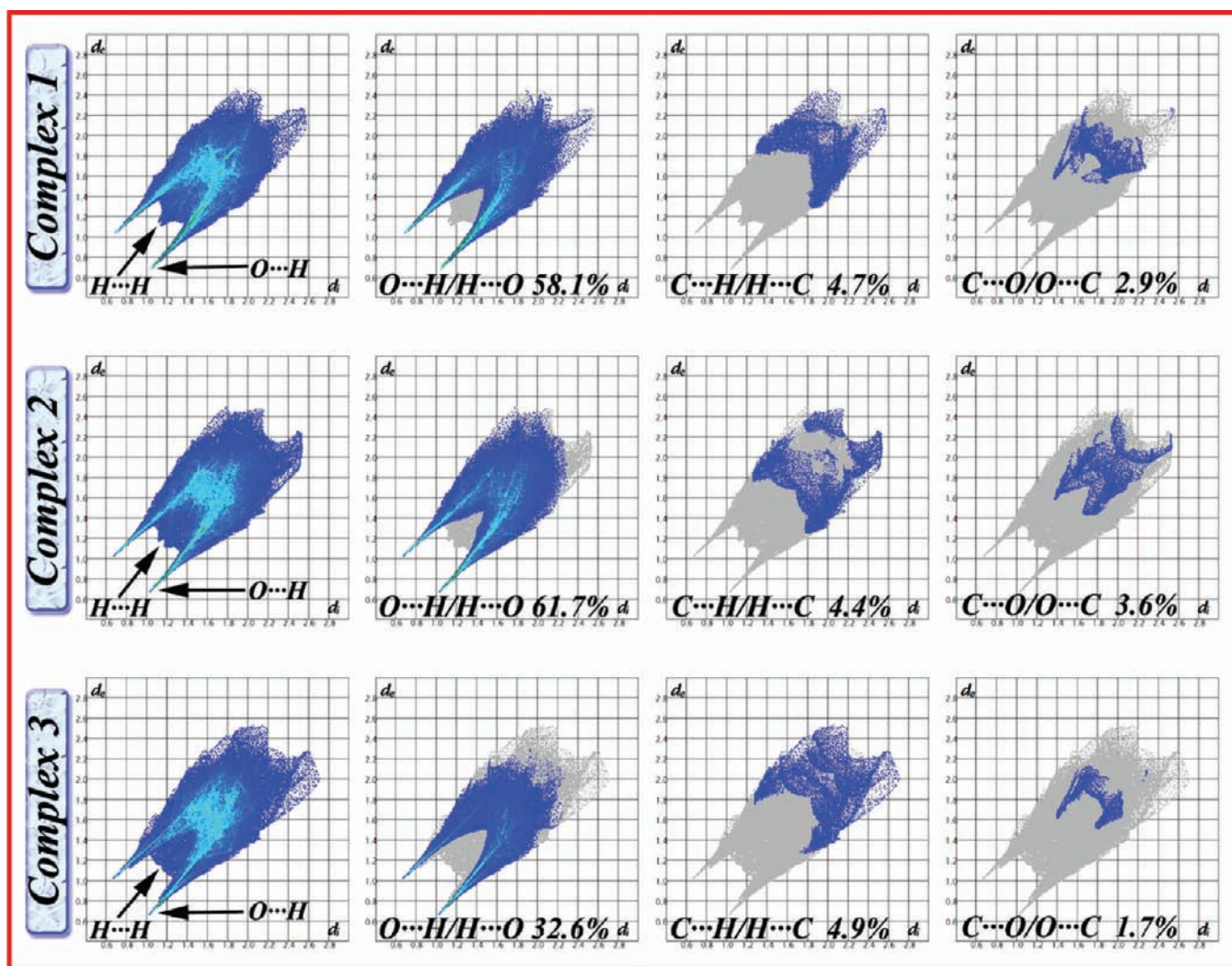


Figure 14. Fingerprint plots. Full (left) and resolved into O...H/H...O, C...H/H...C, and O...H/H...O contacts (right) for the title complexes.

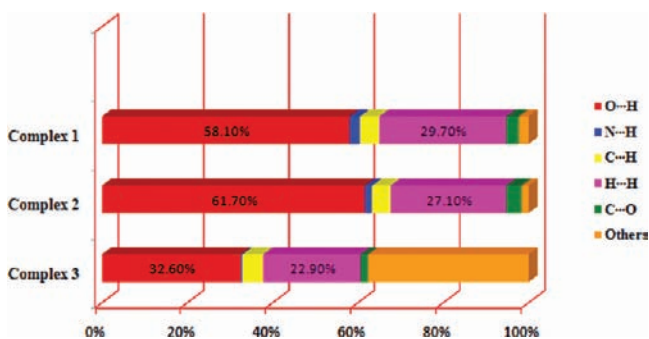


Figure 15. Relative contributions of various intermolecular contacts to the Hirshfeld surface area in 1–3.

and previously mentioned herein, this interaction can be described as a double lp- π interaction, where the lp belongs to the nitrogen atom of the amino group. Since three different types of noncovalent interactions are established in the assemblies, we have evaluated them in order to know which one is responsible for the differences in the formation energies.

To measure the contributions of the different interactions to the total binding energies, we have computed the reactions shown in Figures 17–19. Some interesting issues can be extracted from the results. First, both lp- π and anion- π interactions are large

and negative. As previously mentioned, the lp- π interaction is very favorable because the carbonyl group that participates in the interaction belongs to an anionic species. For nitrate (1), the anion- π interaction is 5.2 kcal/mol more favorable than the lp- π interaction (Figure 17). Interestingly, for perchlorate (2), both interactions are almost isoenergetic (~ 71 kcal/mol; Figure 18), and for hexafluorophosphate (3), the lp- π interaction is 4.9 kcal/mol (Figure 19) more favorable than the anion- π . Second, for all compounds 1–3, the strength of the lp- π interaction is almost constant, and the difference is mainly observed in the anion- π interaction. Therefore, the differences observed in the formation energies of the assemblies (see Figure 16) mainly reflect differences in the anion- π interaction strength. The interaction energies of 1–3 follow the same trend as the equilibrium distances. The differences in interaction energies can be explained in terms of the geometry of the anion. Since the three anions are monoanionic, the negative charge is shared by three oxygen atoms in 1, by four in 2, and by six fluorine atoms in 3. Since the interaction is mainly characterized by the participation of a single atom of the polyatomic anion, the interaction is progressively weakened on going from 1 to 3.

Another interesting point that we have analyzed is the energetic features of the repulsive $\pi^+-\pi^+$ interaction of the assemblies,

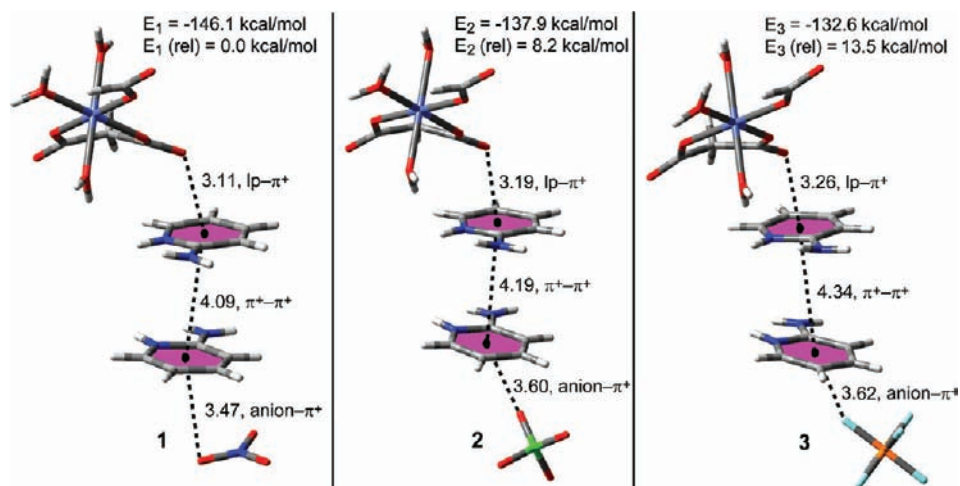


Figure 16. Formation energies and geometric features of the lone pair- π/π - π /anion- π assemblies in compounds 1–3.

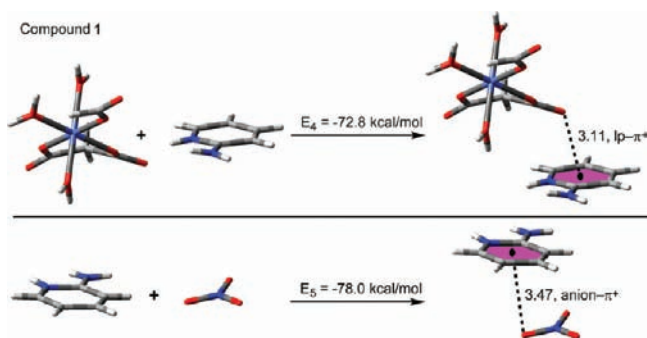


Figure 17. Equations used to measure interaction energies E_4 and E_5 in compound 1. Distances are in Å.

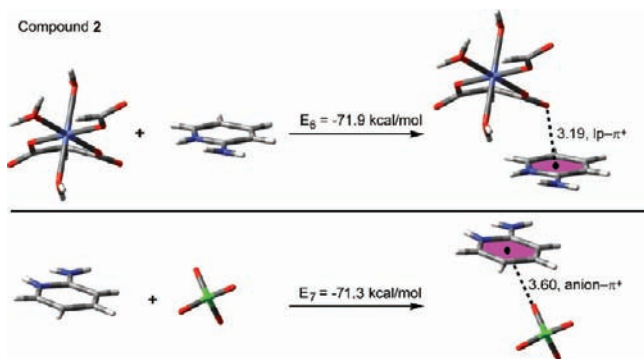


Figure 18. Equations used to measure interaction energies E_6 and E_7 in compound 2. Distances are in Å.

which is largely compensated by the strength of the anion- π and lp- π interactions, as demonstrated by the very favorable formation energies computed for the assemblies. To evaluate this interaction, we have computed the formation energies of the assemblies considering that the anion- π and lp- π complexes have been previously formed (see Figure 20). The interaction energies are indicated in Figure 20 (E_{10} – E_{12}), and as anticipated, they are repulsive. Unexpectedly, the energies are very small (<6.2 kcal/mol), indicating that the presence of the counterions largely reduces the electrostatic repulsion of the positively charged aminopyridine moieties. In addition, the double lp- π interaction that is formed in this special type of stacking also contributes to reducing the electrostatic repulsion.

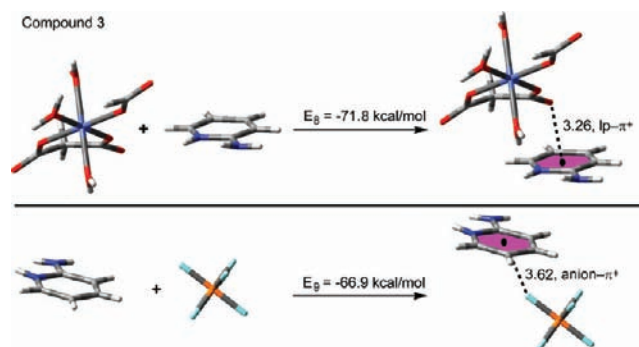


Figure 19. Equations used to measure interaction energies E_8 and E_9 in compound 3. Distances are in Å.

Finally, we have performed the AIM analysis of the assemblies in order to visualize and characterize the noncovalent interactions that stabilize them. In Figure 21, we show the distribution of critical points that characterize the different interactions and the bond paths connecting the different atoms of the interacting parts by means of the bond critical points. For compounds 1–3, the lp- π^+ interaction is characterized by the presence of one bond critical point connecting one oxygen atom of the malonate with one nitrogen atom of the aromatic ring. Moreover, the π^+ - π^+ interaction is characterized by the presence of four bond critical points that connect four atoms of one aminopyridine moiety with four atoms of the other one. The interaction is further characterized by the presence of several ring and cage critical points. In compound 1, the anion- π^+ interaction is characterized by the presence of two bond critical points that connect one oxygen atom of the nitrate with two atoms of the aminopyridine ring (see Figure 21). As a consequence, a ring critical point is also generated. In 2 and 3, the anion- π^+ interaction is characterized by the presence of two bond critical points that connect two oxygen or fluorine atoms of the anion with one carbon atom of the ring. In both complexes, the interaction is further characterized by a ring critical point. Last, we have analyzed in compound 2 the long anion- π^+ interaction (represented in the complex denoted as π^+ -anion- π^+). The AIM analysis confirms that this interaction exists, and it is characterized by a single critical point that connects one oxygen atom of the perchlorate ion with one carbon atom of the ring.

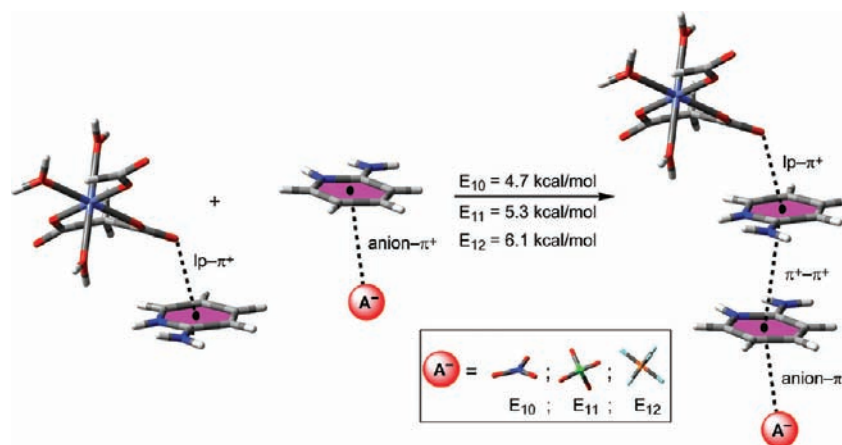


Figure 20. Equation used to measure the interaction energies E_{10} – E_{12} in compounds 1–3.

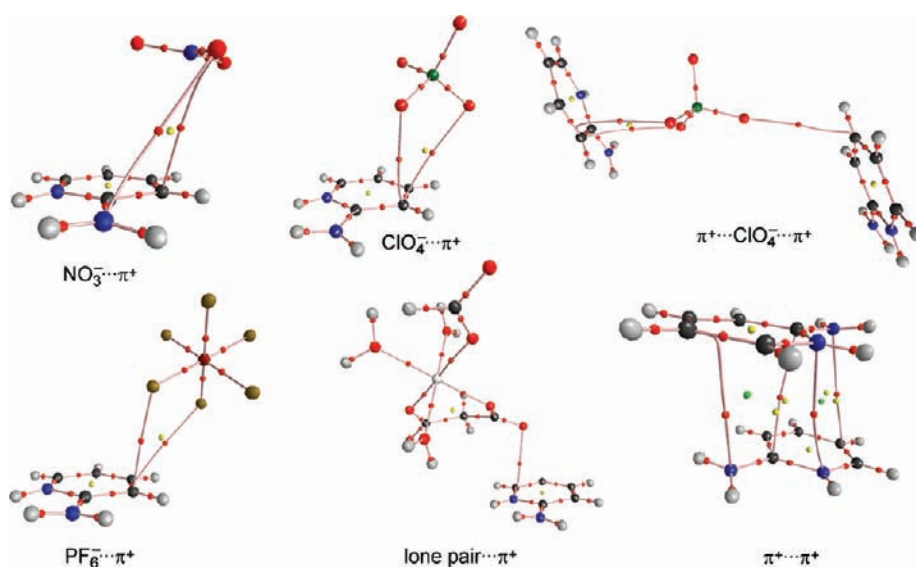


Figure 21. Distribution of critical points in the assemblies of compounds 1–3. Bond, ring, and cage critical points are represented by red, yellow, and green spheres, respectively. The bond paths connecting nuclei and bond critical points are also represented.

CONCLUSIONS

To sum up, the three Co(II) coordination compounds synthesized having malonate as the primary ligand and protonated 2-aminopyridine as the auxiliary ligands acting as the counteranion in each, with nitrate, perchlorate, or hexafluorophosphate as counteranions, are structurally examined along with Hirshfeld surface analyses and DFT studies to confirm the existence and compare the energetics of the supramolecular interactions involving π systems of immense importance like lone pair– π and anion– π .^{3,6} In the solid-state structure of the perchlorate complex, we see a unique combination of weak forces, *viz.* lone pair– π / π – π / π – π –anion– π / π –lone pair interactions, that contributes to the self-assembly process, which has only two previous examples so far known.^{7fg} However, the observed network in the structures of nitrate and hexafluorophosphate compounds that we examined until now arises due to lone pair– π / π – π / π –anion associations.^{7a,c,g,h} These complexes clearly show how important the counteranion is in 2D and 3D packing of metal organic hybrid frameworks by the formation of extended supramolecular networks. It is also interesting that nitrate and hexafluorophosphate become attached to electron deficient aminopyridinium cations in the same fashion, whereas perchlorate used multiple arms for the

same purpose and generated a different network than the others. For perchlorate complexes, it is also noteworthy that only in the case of the Mg complex did this anion enjoy a minimum separation and because of which unusual perchlorate–perchlorate interactions resulted in the creation of 2D sheets.^{7f} A question instantly appears: why does perchlorate behave so differently? We are currently continuing to investigate this by synthesizing closely comparable compounds and performing thorough and comprehensive DFT studies. Lone pair– π and anion– π forces are omnipresent in chemical and biological systems including anion recognition studies.^{3,6} It is understood that such interactions coupled with π – π forces will receive more attention in the coming years with a hunt for further experimental and theoretical studies to uncover the mechanistic aspects of chemical reactions in biological processes including proton coupled electron transfers that are often associated with enzymatic redox reactions.²⁴ An in depth understanding of such weak forces, particularly in their associative fashion, should thus be considered essential.

ASSOCIATED CONTENT

Supporting Information

X-ray crystallographic data in CIF format for 1, 2, and 3 (CCDC Nos. 849012, 849013, and 849014 respectively for 1, 2, and 3).

This material is available free of charge via the Internet at <http://pubs.acs.org>.

AUTHOR INFORMATION

Corresponding Author

*E-mail: som_rc_ju@yahoo.co.in (S.R.C.); smukhopadhyay@chemistry.jdvu.ac.in (S.M.).

Notes

The authors declare no competing financial interest.

ACKNOWLEDGMENTS

P.M. thanks the Council of Scientific and Industrial Research (New Delhi, India) for a Junior Research Fellowship (09/096 (0641) 2010-EMR-I). A.D. gratefully acknowledges the University Grants Commission (New Delhi) for a research fellowship under the scheme "UGC Research Fellowship in Science for Meritorious Students 2007–2008". A.F. thanks CONSOLIDER–Ingenio 2010 (CSD2010-0065) and the MICINN of Spain (project CTQ2011-27512/BQU, FEDER funds) for financial support. S.M. is grateful to the PURSE programme in the Department of Chemistry, Jadavpur University for financial support of this work.

REFERENCES

- (1) (a) Steed, J. W.; Atwood, J. L. *Supramolecular Chemistry*; John Wiley & Sons, Ltd: Chichester, U. K., 2000. (b) Schneider, H.-J. *Angew. Chem., Int. Ed.* **2009**, *48*, 3924. (c) Meyer, E. A.; Castellano, R. K.; Diederich, F. *Angew. Chem., Int. Ed.* **2003**, *42*, 1210. (d) Dougherty, D. A. *Science* **1996**, *271*, 163. (e) Kim, K. S.; Tarakeswar, P.; Lee, J. Y. *Chem. Rev.* **2000**, *100*, 4145. (f) Lee, E. C.; Kim, D.; Jureeká, P.; Tarakeswar, P.; Hobza, P.; Kim, K. S. *J. Phys. Chem. A* **2007**, *111*, 3446. (g) Reddy, A. S.; Sastry, G. N. *J. Phys. Chem. A* **2005**, *109*, 8893. (h) Černý, J.; Hobza, P. *Phys. Chem. Chem. Phys.* **2007**, *9*, 5291. (i) Rappé, A. K.; Bernstein, E. R. *J. Phys. Chem. A* **2000**, *104*, 6117. (j) Hesselmann, A.; Jansen, G.; Schütz, M. *J. Am. Chem. Soc.* **2006**, *128*, 11730. (k) Piacenza, M.; Grimme, S. *Chem. Phys. Chem* **2005**, *6*, 1554. (l) Singh, N. J.; Min, S. K.; Kim, D. Y.; Kim, K. S. *J. Chem. Theory Comput.* **2009**, *5*, 515–529. (m) Bloom, J. W. G.; Wheeler, S. E. *Angew., Chem. Int. Ed.* **2011**, *50*, 7847–7849.
- (2) (a) Schottel, B. L.; Chifotides, H. T.; Dunbar, K. R. *Chem. Soc. Rev.* **2008**, *37*, 68. (b) Ballester, P. *Struct. Bonding (Berlin)* **2008**, *129*, 127. (c) Hay, B. P.; Bryantsev, V. S. *Chem. Commun.* **2008**, 2417. (d) Rosokha, S. V.; Kochi, J. K. *Struct. Bonding (Berlin)* **2008**, *126*, 137. (e) Gamez, P.; Mooibroek, T. J.; Teat, S. J.; Reedijk, J. *Acc. Chem. Res.* **2007**, *40*, 435. (f) Kim, D. Y.; Singh, N. J.; Kim, K. S. *J. Chem. Theory Comput.* **2008**, *4*, 1401–1407. (g) Kim, D.; Tarakeswar, P.; Kim, S. K. *J. Phys. Chem. A* **2004**, *108*, 1250–1258. (h) Chifotides, H. T.; Schottel, B. L.; Dunbar, K. R. *Angew. Chem., Int. Ed.* **2010**, *49*, 7202–7207. (i) Senchyk, G. A.; Lysenko, A. B.; Naumov, D. Y.; Fedin, V. P.; Krautscheid, H.; Domasevitch, K. V. *Inorg. Chem. Commun.* **2010**, *13*, 1576–1579. (j) Müller, M.; Albrecht, M.; Sackmann, J.; Hoffmann, A.; Dierkes, F.; Valkonen, A.; Rissanen, K. *Dalton Trans.* **2010**, *39*, 11329–11334. (k) Costa, J. S.; Castro, A. G.; Pievo, R.; Roubeau, O.; Modéc, B.; Kozlevčar, B.; Teat, S. J.; Gamez, P.; Reedijk, J. *Cryst. Eng. Commun.* **2010**, *12*, 3057–3064. (l) Estarellas, C.; Frontera, A.; Quiñonero, D.; Deyà, P. M. *J. Phys. Chem. A* **2011**, *115*, 7849–7857. (m) Cadman, C. J.; Croft, A. K. *Beilstein J. Org. Chem.* **2011**, *7*, 320–328. (n) Estarellas, C.; Frontera, A.; Quiñonero, D.; Deyà, P. M. *Angew. Chem., Int. Ed. Engl.* **2011**, *50*, 415. (o) Jones, S. G.; Yau, H. M.; Davies, E.; Hook, J. M.; Youngs, T. G. A.; Harper, J. B.; Croft, A. K. *Phys. Chem. Chem. Phys.* **2010**, *12*, 1873. (p) Quiñonero, D.; Deyà, P. M.; Carranza, M. P.; Rodríguez, A. M.; Jalón, F. A.; Manzano, B. R. *Dalton Trans.* **2010**, *39*, 794. (q) Garau, C.; Frontera, A.; Quiñonero, D.; Russo, N.; Deyà, P. M. *J. Chem. Theory Comput.* **2011**, *7*, 3012–3018. (r) Frontera, A.; Quiñonero, D.; Deyà, P. M. *WIREs: Comput. Mol. Sci.* **2011**, *1*, 440. (s) Estarellas, C.; Frontera, A.; Quiñonero, D.; Deyà, P. M. *Chem. Asian J.* **2011**, *6*, 2316–2318. (t) Jeffery, T. D. *Nature Chem.* **2010**, *2*, 516–517. (u) Frontera, A.; Gamez, P.; Mascals, M.; Mooibroek, T. J.; Reedijk, J. *Angew. Chem., Int. Ed.* **2011**, *50*, 9564–9583.
- (3) (a) Mooibroek, T. J.; Gamez, P.; Reedijk, J. *CrystEngComm* **2008**, *10*, 1501. (b) Egli, M.; Sarkhel, S. *Acc. Chem. Res.* **2007**, *40*, 197. (c) Jain, A.; Purohit, C. S.; Verma, S.; Sankaramakrishnan, R. *J. Phys. Chem. B* **2007**, *111*, 8680–8683. (d) Sarkhel, S.; Rich, A.; Egli, M. *J. Am. Chem. Soc.* **2003**, *125*, 8998–8999. (e) Ran, J.; Hobza, P. *J. Chem. Theory Comput.* **2009**, *5*, 1180–1185. (f) Jain, A.; Ramanathan, V.; Sankaramakrishnan, R. *Protein Sci.* **2009**, *18*, 595–605. (g) Lu, Z.; Gamez, P.; Mutikainen, I.; Turpeinen, U.; Reedijk, J. *Cryst. Growth Des.* **2007**, *7*, 1669–1671. (h) Barceló-Oliver, M.; Estarellas, C.; García-Raso, A.; Terrón, A.; Frontera, A.; Quiñonero, D.; Molins, E.; Deyà, P. M. *CrystEngComm.* **2010**, *12*, 362–365. (i) Bushuev, M. B.; Krivopalov, V. P.; Pervukhina, N. V.; Naumov, D. Y.; Moskalenko, G. G.; Vinogradova, K. A.; Sheludyakova, L. A.; Larionov, S. V. *Inorg. Chim. Acta* **2010**, *363*, 1547–1555. (j) Estarellas, C.; Frontera, A.; Quiñonero, D.; Deyà, P. M. *Cent. Eur. J. Chem.* **2011**, *9*, 25–34.
- (4) (a) Quiñonero, D.; Garau, C.; Rotger, C.; Frontera, A.; Ballester, P.; Costa, A.; Deyà, P. M. *Angew. Chem., Int. Ed.* **2002**, *41*, 3389–3392. (b) Quiñonero, D.; Garau, C.; Frontera, A.; Ballester, P.; Costa, A.; Deyà, P. M. *Chem. Phys. Lett.* **2002**, *359*, 486–492. (c) Mascas, M. L.; Armstrong, A.; Bartberger, M. D. *J. Am. Chem. Soc.* **2002**, *124*, 6274–6276. (d) Alkorta, I.; Rozas, I.; Elguero, J. *J. Am. Chem. Soc.* **2002**, *124*, 8593–8598. (e) Frontera, A.; Sączewski, F.; Gdaniec, M.; Dziemidowicz-Borys, E.; Kurland, A.; Deyà, P. M.; Quiñonero, D.; Garau, C. *Chem.—Eur. J.* **2005**, *11*, 6560–6567. (f) García-Raso, A.; Alberti, F. M.; Fiol, J. J.; Tasada, A.; Barceló-Oliver, M.; Molins, E.; Escudero, D.; Frontera, A.; Quiñonero, D.; Deyà, P. M. *Inorg. Chem.* **2007**, *46*, 10724–10735.
- (5) (a) Domasevitch, K. V.; Gural'skiy, I. A.; Solntsev, P. V.; Rusanov, E. B.; Krautscheid, H.; Howard, J. A. K.; Chernega, A. N. *Dalton Trans.* **2007**, 3140–3148. (b) Gural'skiy, I. A.; Solntsev, P. V.; Krautscheid, H.; Domasevitch, K. V. *Chem. Commun.* **2006**, 4808–4810. (c) Mooibroek, T. J.; Black, C. A.; Gamez, P.; Reedijk, J. *Cryst. Growth Des.* **2008**, *8*, 1082–1093. (d) Schottel, B. L.; Chifotides, H. T.; Shatruk, M.; Chouai, A.; Perez, L. M.; Bacsá, J.; Dunbar, K. R. *J. Am. Chem. Soc.* **2006**, *128*, 5895–5912. (e) Dawson, R. E.; Hennig, A.; Weimann, D. P.; Emery, D.; Ravikumar, V.; Montenegro, J.; Takeuchi, T.; Gabutti, S.; Mayor, M.; Mareda, J.; Schalley, C. A.; Matile, S. *Nat. Chem.* **2010**, *2*, 533–538. (f) Hadlington, S. *Chem. World* **2010**, <http://www.rsc.org/chemistryworld/News/2010/May/16051001.asp>. (g) Cresswell, A. L.; Piepenbrock, M. O. M.; Steed, J. W. *Chem. Commun.* **2010**, *46*, 2787–2789. (h) Sawada, T.; Fujita, M. *J. Am. Chem. Soc.* **2010**, *132*, 7194–7201.
- (6) Robertazzi, A.; Krull, F.; Knapp, E.-W.; Gamez, P. *CrystEngComm* **2011**, *13*, 3293–3300.
- (7) (a) Choudhury, S. R.; Gamez, P.; Robertazzi, A.; Chen, C. Y.; Lee, H. M.; Mukhopadhyay, S. *Cryst. Growth Des.* **2008**, *8*, 3773–3784. (b) Choudhury, S. R.; Chen, C. Y.; Seth, Kar, S. T.; Lee, H. M.; Colacio, E.; Mukhopadhyay, S. *J. Coord. Chem.* **2009**, *62*, 540–551. (c) Choudhury, S. R.; Dey, B.; Das, S.; Gamez, P.; Robertazzi, A.; Chan, K. T.; Lee, H. M.; Mukhopadhyay, S. *J. Phys. Chem. A* **2009**, *113*, 1623–1627. (d) Choudhury, S. R.; Dey, B.; Das, S.; Robertazzi, A.; Jana, A. D.; Chen, C. Y.; Lee, H. M.; Gamez, P.; Mukhopadhyay, S. *Dalton Trans.* **2009**, 7617–7624. (e) Choudhury, S. R.; Lee, H. M.; Hsiao, T. H.; Colacio, E.; Jana, A. D.; Mukhopadhyay, S. *J. Mol. Struct.* **2010**, *967*, 131–139. (f) Das, A.; Choudhury, S. R.; Dey, B.; Yalamanchili, S. K.; Helliwell, M.; Gamez, P.; Mukhopadhyay, S.; Estarellas, C.; Frontera, A. *J. Phys. Chem. B* **2010**, *114*, 4998–5009. (g) Das, A.; Choudhury, S. R.; Estarellas, C.; Dey, B.; Frontera, A.; Hemming, J.; Helliwell, M.; Gamez, P.; Mukhopadhyay, S. *CrystEngComm.* **2011**, *13*, 4519–4527. (h) Das, A.; Choudhury, S. R.; Manna, P.; Baxter, D.; Helliwell, M.; Mukhopadhyay, S. *Polyhedron* **2011**, *30*, 2121–2126.
- (8) Spackman, M. A.; McKinnon, J. J. *CrystEngComm.* **2002**, *4*, 378–392.

(9) (a) McKinnon, J. J.; Jayatilaka, D.; Spackman, M. A. *Chem. Commun.* **2007**, 3814–3816. (b) Spackman, M. A.; McKinnon, J. J.; Jayatilaka, D. *CrystEngComm* **2008**, *10*, 377–388. (c) Spackman, M. A.; Jayatilaka, D. *CrystEngComm* **2009**, *11*, 19–32. (d) Hirshfeld, F. L. *Theor. Chim. Acta* **1977**, *44*, 129–138. (e) Clausen, H. F.; Chevallier, M. S.; Spackman, M. A.; Iversen, B. B. *New J. Chem.* **2010**, *34*, 193–199. (f) Martin, A. D.; Hartlieb, K. J.; Sobolev, A. N.; Raston, C. L. *Cryst. Growth Des.* **2010**, *10*, 5302–5306.

(10) (a) Seth, S. K.; Saha, N. C.; Ghosh, S.; Kar, T. *Chem. Phys. Lett.* **2011**, *506*, 309–314. (b) Seth, S. K.; Sarkar, D.; Kar, T. *CrystEngComm* **2011**, *13*, 4528–4535. (c) Seth, S. K.; Sarkar, D.; Roy, A.; Kar, T. *CrystEngComm* **2011**, *13*, 6728–6741. (d) Seth, S. K.; Saha, I.; Estarellas, C.; Frontera, A.; Kar, T.; Mukhopadhyay, S. *Cryst. Growth Des.* **2011**, *11*, 3250–3265. (e) Seth, S. K.; Sarkar, D.; Jana, A. D.; Kar, T. *Cryst. Growth Des.* **2011**, *11*, 4837–4849.

(11) (a) Rohl, A. L.; Moret, M.; Kaminsky, W.; Claborn, K.; McKinnon, J. J.; Kahr, B. *Cryst. Growth Des.* **2008**, *8*, 4517–4525. (b) Parkin, A.; Barr, G.; Dong, W.; Gilmore, C. J.; Jayatilaka, D.; McKinnon, J. J.; Spackman, M. A.; Wilson, C. C. *CrystEngComm* **2007**, *9*, 648–652.

(12) Sheldrick, G. M. *Acta Crystallogr., Sect. A* **2008**, *64*, 112–122.

(13) (a) Spackman, M. A.; Byrom, P. G. *Chem. Phys. Lett.* **1997**, *267*, 215–220. (b) McKinnon, J. J.; Mitchell, A. S.; Spackman, M. A. *Chem.—Eur. J.* **1998**, *4*, 2136–2141.

(14) McKinnon, J. J.; Spackman, M. A.; Mitchell, A. S. *Acta Crystallogr. Sect. B* **2004**, *60*, 627–668.

(15) Wolff, S. K.; Grimwood, D. J.; McKinnon, J. J.; Jayatilaka, D.; Spackman, M. A. *Crystal Explorer 2.1*; University of Western Australia: Perth, Australia, 2007.

(16) Koenderink, J. J.; van Doorn, A. J. *Image Vision Comput.* **1992**, *10*, 557–564.

(17) Frisch, M. J.; Trucks, G. W.; Schlegel, H. B.; Scuseria, G. E.; Robb, M. A.; Cheeseman, J. R.; Scalmani, G.; Barone, V.; Mennucci, B.; Petersson, G. A.; Nakatsuji, H.; Caricato, M.; Li, X.; Hratchian, H. P.; Izmaylov, A. F.; Bloino, J.; Zheng, G.; Sonnenberg, J. L.; Hada, M.; Ehara, M.; Toyota, K.; Fukuda, R.; Hasegawa, J.; Ishida, M.; Nakajima, T.; Honda, Y.; Kitao, O.; Nakai, H.; Vreven, T.; Montgomery, J. A., Jr.; Peralta, J. E.; Ogliaro, F.; Bearpark, M.; Heyd, J. J.; Brothers, E.; Kudin, K. N.; Staroverov, V. N.; Kobayashi, R.; Normand, J.; Raghavachari, K.; Rendell, A.; Burant, J. C.; Iyengar, S. S.; Tomasi, J.; Cossi, M.; Rega, N.; Millam, N. J.; Klene, M.; Knox, J. E.; Cross, J. B.; Bakken, V.; Adamo, C.; Jaramillo, J.; Gomperts, R.; Stratmann, R. E.; Yazyev, O.; Austin, A. J.; Cammi, R.; Pomelli, C.; Ochterski, J. W.; Martin, R. L.; Morokuma, K.; Zakrzewski, V. G.; Voth, G. A.; Salvador, P.; Dannenberg, J. J.; Dapprich, S.; Daniels, A. D.; Farkas, Ö.; Foresman, J. B.; Ortiz, J. V.; Cioslowski, J.; Fox, D. *Gaussian 09*; Gaussian Inc.: Wallingford, CT, 2009.

(18) Zhao, Y.; Truhlar, D. G. *Theor. Chem. Acc.* **2008**, *120*, 215–241.

(19) Bader, R. F. W. *Atoms in Molecules—A Quantum Theory*; Oxford University Press: Oxford, U. K., 1990.

(20) (a) Bader, R. F. W. *Chem. Rev.* **1991**, *91*, 893. (b) Grabowski, S. J.; Pfitzner, A.; Zabel, M.; Dubis, A. T.; Palusiak, M. *J. Phys. Chem. B* **2004**, *108*, 1831. (c) Vila, A.; Mosquera, R. A. *THEOCHEM* **2001**, *546*, 63. (d) Chopra, D.; Cameron, T. S.; Ferrara, J. D.; Guru Row, T. N. *J. Phys. Chem. A* **2006**, *110*, 10465.

(21) (a) Delgado, F. S.; Hernández-Molina, M.; Sanchiz, J.; Ruiz-Pérez, C.; Rodríguez-Martín, Y.; López, T.; Lloret, F.; Julve, M. *CrystEngComm* **2004**, *6*, 106–111. (b) Das, A.; Dey, B.; Jana, A. D.; Hemming, J.; Helliwell, M.; Lee, H. M.; Hsiao, T.-H.; Suresh, E.; Colacio, E.; Choudhury, S. R.; Mukhopadhyay, S. *Polyhedron* **2010**, *29*, 1317–1325.

(22) (a) Pasan, J.; Sanchiz, J.; Lloret, F.; Julve, M.; Ruiz-Pérez, C. *CrystEngComm* **2007**, *9*, 478–487 and references therein. (b) Delgado, F. S.; Lahoz, F.; Lloret, F.; Julve, M.; Ruiz-Pérez, C. *Cryst. Growth Des.* **2008**, *8*, 3219–3232.

(23) Bondi, A. J. *J. Phys. Chem.* **1964**, *68*, 441–451.

(24) DiLabio, G. A.; Johnson, E. R. *J. Am. Chem. Soc.* **2007**, *129*, 6199–6203.